machines

Article

Numerical Investigation of the Actual Volumetric Flow Rate and Volumetric Efficiency and Optimization of the Geometric Parameters of a Three-Rotor Pump with Lantern Meshing—Part II

Ivaylo Nikolaev [1], Ivan Georgiev [2,3], Slavi Georgiev [2,3,*] and Georgi Iliev [4]

[1] Department of Heat, Hydraulics and Environmental Engineering, Agrarian and Industrial Faculty, University of Ruse, 8 Studentska Str., 7004 Ruse, Bulgaria; nikolaev@uni-ruse.bg
[2] Department of Applied Mathematics and Statistics, Faculty of Natural Sciences and Education, University of Ruse, 8 Studentska Str., 7004 Ruse, Bulgaria; irgeorgiev@uni-ruse.bg
[3] Department of Information Modeling, Institute of Mathematics and Informatics, Bulgarian Academy of Sciences, 8 Acad. Georgi Bonchev Str., 1113 Sofia, Bulgaria
[4] Department of Power Engineering, Faculty of Mechanical and Precision Engineering, Technical University of Gabrovo, 4 Hadzhi Dimitar Str., 5300 Gabrovo, Bulgaria; g.iliev@tugab.bg
* Correspondence: sggeorgiev@uni-ruse.bg; Tel.: +359-82-888-623

Abstract

Part II of this study builds upon the mathematical framework developed and validated in Part I for describing the geometry and volumetric performance indicators of an innovative three-rotor hydraulic pump with bilateral lantern meshing. This part focuses on the numerical investigation and multi-objective optimization of these indicators through the proper selection of geometric parameters. The aim of the study is to establish the isolated and combined influence of the dimensionless geometric parameters—number of teeth z, relative lantern radius r_c^*, and cycloid shortening coefficient λ—on the actual flow rate Q and the volumetric efficiency η_v under various operating conditions, while maintaining the overall dimensions of the pump element in the radial and axial directions. Through detailed numerical analysis and subsequent rigorous analytical proof, it has been established that the optimal values of the geometric coefficients $r_{c,opt}^*$ and λ_{opt} are strictly determined and provide a simultaneous global maximization of both indicators (Q, η_v), regardless of the operating pressure p, rotational speed n, or the viscosity of the working fluid. However, an analytically irresolvable conflict regarding the number of teeth z has been identified: a small number maximizes the flow rate, whereas a large number increases the volumetric efficiency. To overcome this contradiction, the problem is formulated within the class of mixed-integer nonlinear programming (MINLP), and multicriteria Pareto optimization is applied, combined with the PSIMS method for the selection of optimal compromise solutions. An empirical relationship (with a coefficient of determination of $R^2 = 0.9603$) has been derived, which defines the optimal number of teeth z_{opt} as a function of the operating pressure and rotational speed. The proposed methodology provides a reliable and applicable tool for designing highly efficient three-rotor pumps tailored to specific operational requirements.

Keywords: three-rotor hydraulic pump; lantern meshing; volumetric efficiency; internal leakages; multi-objective Pareto optimization; mixed-integer nonlinear programming (MINLP); PSIMS selection; mathematical modeling

Academic Editors: Paweł Śliwiński, Piotr Osiński, Mykola Karpenko and Pedro Javier Gamez-Montero

Received: 18 March 2026
Revised: 20 June 2026
Accepted: 22 June 2026
Published: 25 June 2026

1. Introduction

The design optimization of gear pumps is the subject of continuous research interest, with contemporary scientific publications showing a tendency toward improving the geometry according to various specific criteria. Among these are the consideration of elastic deformations of the housing and their influence on the working clearances [1], the application of Navier–Stokes solutions for describing unsteady flows under variable pressure gradients [2], the minimization of peak pressures caused by the "trapped volume" problem under highly constrained conditions [3], etc. To solve such problems, specialized software tools for numerical simulations are often used, such as the HYGESim model [4]. This type of software solution usually relies on simulation-based optimization, coupling lumped-parameter hydraulic models with iterative search algorithms. These iterative simulation approaches have proven effective for achieving high-accuracy results in the analysis of classical gear pumps, but at the same time they require considerable computational resources and a previously known, established geometry.

In contrast, although computational fluid dynamics (CFD) methods and numerical modeling are theoretically applicable, their direct use for the purposes of multiparametric geometric optimization in conceptually new developments, such as the innovative three-rotor pump with cycloidal (lantern) meshing considered here, is computationally inefficient. 3D CFD simulations require the generation of a computational mesh for each specific configuration, which makes the exploration of the vast space of possible geometries unjustified in terms of time. In the contemporary scientific literature, this problem is effectively overcome through the application of dimensional analysis, established in the fundamental theory of positive-displacement machines [5]. Today, this classical approach successfully replaces computationally intensive CFD simulations in the precise modeling of leakage flows in the clearances of gear machines [6]. In parallel, similarity theory has become established as a powerful tool for reducing the parametric space in the evaluation of the energy efficiency of fluid machines [7]. The generalized criterion equations derived through dimensional analysis are increasingly used as reliable objective functions in solving optimization problems [8] and as an input basis for advanced algorithms, bypassing resource-intensive numerical simulations [9]. Unlike iterative simulation approaches, a direct analytical method based on the criterion equations derived in Part I [10] is applied here. This approach allows not only the description of volumetric losses based on real experimental data but also provides the possibility of conducting a rigorous mathematical investigation that can serve as a basis for multicriteria geometric optimization.

In the first part [10] of the present study, the fundamental mathematical apparatus for evaluating the pump characteristics was developed and validated. By integrating mathematical modeling, similarity theory, and dimensional analysis, the objective functions were refined and empirical relationships were derived for the actual volumetric flow rate Q and the volumetric efficiency η_v. While Part I successfully defined the domain of geometric existence of the gear and established the necessary theoretical basis, the actual determination of the optimal geometric configuration requires conducting an in-depth numerical and analytical investigation to reveal and balance the complex interrelationships among the individual geometric parameters of the pump. At the present stage of the study, it is necessary to resolve the critical conflict between maximizing the working displacement and minimizing volumetric leakages—a task that requires the application of specialized optimization tools.

Resolving this conflict requires the selection of an appropriate optimization method. Various approaches are applied in the contemporary literature, each with its own advantages and limitations. Gradient-based methods, including steepest-descent, multiple-gradient, and related schemes [11–14], are effective for smooth differentiable formulations, but they are sensitive to local extrema and are not always the most convenient choice

https://doi.org/10.3390/machines14070720

in the presence of discrete design variables and nonconvexities [15–18]. Neural networks and surrogate models [19–25], on the other hand, successfully approximate complex nonlinear relationships and accelerate the exploration of the parameter space, but they require an extensive training stage and do not independently resolve the conflict between multiple criteria. Stochastic and quasi-Monte Carlo approaches [26–29] are powerful numerical methods for the global exploration of the parameter space and for sensitivity analysis [28–31], using, respectively, random and low-discrepancy-generated samples for the efficient investigation of multidimensional models [31,32]. However, by themselves they do not provide a direct mechanism for selection under multicriteria conflicts. Owing to the well-known conflict between flow rate and volumetric losses, as well as the mixed structure of the variables, involving continuous geometric parameters and a discrete number of teeth, the methods of mixed-integer nonlinear programming (MINLP) and multicriteria Pareto optimization [33–41] emerge as the most promising theoretical apparatus for achieving an engineering-interpretable compromise.

In this regard, the present paper represents a logical continuation (Part II) of the research work, the main objective of which is: To conduct a systematic numerical and analytical investigation for optimizing the geometric parameters of a three-rotor pump with cycloidal meshing with a view to maximizing its objective functions—the actual volumetric flow rate Q and the volumetric efficiency η_v. On this basis, multicriteria Pareto optimization is performed to determine the optimal geometric configuration depending on the specific operating regimes and the properties of the working fluid.

To achieve this general objective, the present work focuses on solving the second main group of tasks from the overall study. Initially, the research process requires conducting a parametric numerical investigation of the influence of the geometric parameters on the output flow characteristics of the pump in order to establish their empirical optima. A key point in the methodology is the implementation of a rigorous analytical proof that these geometric optima are global strictly within the space of the two considered objective functions, namely the actual flow rate and the volumetric efficiency, with respect to all independent variables, which guarantees their validity under arbitrary operating regimes and numbers of teeth.

The next phase of the work is directed toward constructing a mathematical model for multicriteria Pareto optimization, formulated as a mixed-integer nonlinear programming (MINLP) problem, in order to resolve the conflict in the selection of the number of teeth z. The implementation of this task includes the generation of Pareto fronts and the ranking of solutions by means of the PSIMS method under different operating conditions. As a final stage, the task is set to derive accessible practical algebraic relationships that may serve as a direct recommendation in the selection of an optimal geometric configuration.

Due to the large volume of the study, the tasks covering the formulation of the objective functions, the definition of the independent variables, and the refinement of the empirical coefficients based on statistical processing of experimental data are presented in detail in Part I. The present Part II is focused entirely on the analytical confirmation of the optima, the multicriteria optimization, and the derivation of the final design relationships.

2. Materials and Methods

In order to ensure the self-contained nature and coherence of the presentation in Part II, the present introduction summarizes the fundamental relationships and definitions established in Part I, which will be used as a basis for the analytical proofs and the optimization procedure. In this regard, it should be additionally recalled that the empirical models used below were calibrated in Part I on the basis of measurements from a physical prototype of the three-rotor pump, tested with Lubrica MH-L 68 hydraulic oil (LUBRICA, Ruse, Bulgaria) at different pressures, rotational speeds, and temperatures. The geometry

https://doi.org/10.3390/machines14070720

of the prototype, the equivalent radial and axial clearances, as well as the temperature-dependent functions for the viscosity and density of the working fluid, were determined from these experimental investigations. Therefore, the numerical investigation and optimization in the present Part II are not based on arbitrarily selected coefficients, but on the experimentally refined relationships derived and validated in Part I.

2.1. Geometric Model and Parameterization

The geometry of the gear is defined by the scale module m and three independent dimensionless parameters: the number of teeth (lanterns) z of the central lantern gear, the relative lantern radius r_c^*, and the cycloid shortening coefficient λ. The relative geometric clearances and thickness are defined, respectively, as:

Relative equivalent radial clearance:

$$\delta_1^* = \frac{\delta_1}{m} \tag{1}$$

Relative equivalent axial clearance:

$$\delta_2^* = \frac{\delta_2}{m} \tag{2}$$

Relative thickness of the gears:

$$b^* = \frac{b}{m} \tag{3}$$

For the experimental prototype, it was established that the scale module m is selected depending on the fixed outer dimension (the root circle diameter of the hypocycloid gear d_{Hf} according to the formula:

$$m = \frac{d_{Hf}}{z+\lambda+2r_c^*} \tag{4}$$

In Part I, it was clarified that the maximum displacement volume and theoretical flow rate are achieved at the optimal point T_{opt}, where the parameters coincide and are calculated by the relationship:

$$r_{c,opt}^* = \lambda_{opt} = \sqrt{\frac{27(z-1)z^2}{27(z-1)z^2+4(z+1)^3}} \tag{5}$$

2.2. Domain of Existence and Constraint Conditions

Designing the pump requires the selected parameters to fall within the Domain of geometric existence, defined by the blocking contour (BC). The system of four constraint inequalities defining the feasible set reduces to the following boundaries:

Epicycloid teeth undercutting boundary:

$$\lambda \le \lambda_{Emax} = \sqrt{1 - \frac{4}{27}\frac{(z+1)^3 (r_c^*)^2}{z^2(z-1)}} \tag{6}$$

Cycloid teeth interference boundary:

$$\lambda \le \lambda_{max} = r_c^* \tag{7}$$

Adjacent lanterns interference boundary:

$$r_c^* < r_{uc}^* = \frac{z}{2}\sin\frac{\pi}{z} \tag{8}$$

Minimum contact ratio boundary

$$\varepsilon_{u,min}\colon \lambda > \lambda_{min} = \frac{\sin[\theta]}{\cos\left(\frac{\pi\varepsilon_{u,min}}{Z}\right)}, \tag{9}$$

where $[\theta]$ is the allowable angle of force transmission between the force $\vec{F}$ acting in the center of the lanterns and the velocity $\vec{v}$ of its application point. For geometric calculations, the following values are recommended: $[\theta] = 30°$ and $\varepsilon_{u,min} = 1.15$ For the precise determination of the displacement volume in Part I, a high-accuracy approximation formula for the displacement volume q (error $\pm 0.18\%$) was selected, expressed through the dimensionless geometric coefficients as:

$$q = \frac{m^3 \cdot b^*}{1000}\left[z(24.95 + 655\lambda + 12.35r_c^* - 2.25z) + \lambda(24.3\lambda - 263) - r_c^*(86 + 186\lambda) - 55.9\right] \tag{10}$$

2.3. Criterion Equation for the Volumetric Efficiency (First Objective Function)

The mathematical model for the volumetric efficiency η_v is based on the similarity theory and is defined by an approximation criterion equation derived from a set of similarity criteria. For its precise formulation, the following dimensionless similarity criteria were introduced:

Euler number for dimensionless pressure:

$$\pi_1 = Eu = \frac{p}{\rho(n \cdot m)^2} \tag{11}$$

Reynolds number for dimensionless viscosity:

$$\pi_2 = Re = \frac{\mu}{\rho \cdot n \cdot m^2} \tag{12}$$

Here, p is the operating pressure of the pump, n is the rotational speed, ρ is the fluid density, and μ is its dynamic viscosity. In order to guarantee the mathematical correctness and strict dimensionlessness of the derived π-criteria, in the theoretical relationships these quantities are defined strictly through their basic SI units: the pressure is in [Pa], the rotational speed is in $[\mathrm{s}^{-1}]$, the density is in $[\mathrm{kg/m^3}]$, the dynamic viscosity is in $[\mathrm{Pa \cdot s}]$, and the scale module m is in [m]. Subsequently, however, in the numerical investigation and in the analytical proofs presented in Appendix A, the dimensions adopted in engineering practice, such as bar, min^{-1}, and mm, are used directly. In order to preserve the dimensionlessness of the criteria during this transition, the corresponding conversion factors are introduced into the equations; see Equations (A2) and (A3). This approach was deliberately chosen for several reasons. First, it allows direct work with the raw experimental data without requiring their preliminary and extensive conversion, which minimizes the risk of computational errors. Second, the use of practical units provides a clearer physical and engineering interpretation of the operating regimes. Finally, it guarantees full consistency with the empirical relationships for the fluid properties calibrated in Part I, Equations (19) and (20), which were derived precisely on the basis of these dimensions.

Since the hydraulic losses in the flow passages of positive-displacement hydraulic machines are negligible [5], the pressure drop in the sealing clearances, on which the volumetric leakages physically depend, practically coincides with the operating pressure of the pump. On this basis, and in order to preserve strict consistency of the notation with Part I, the parameter p is used directly here. In the same place, the area S_n and the hydraulic diameter d_s of the total equivalent clearance are also defined, as well as their dimensionless (relative) quantities S_n^* and d_s^*, as follows:

$$S_n^* = 3\delta_1^* b^* + \delta_2^*[\pi(z + \lambda) + 2(2 + \pi)r_c^*] \tag{13}$$

$$d_s^* = \frac{2\{3\delta_1^* b^* + \delta_2^*[\pi(z+\lambda) + 2(2+\pi)r_c^*]\}}{3(\delta_1^* + b^*) + 4\delta_2^* + \pi(z+\lambda) + 2(2+\pi)r_c^*} \tag{14}$$

The relationship between the relative and absolute values of these parameters is as follows:

$$S_n^* = \frac{S_n}{m^2}; \quad d_s^* = \frac{d_s}{m} \tag{15}$$

The generalized dimensionless geometric coefficient K, combining all geometric parameters of the meshing, is defined through the dimensionless displacement volume $q^* = \mathrm{q/m^3}$ as:

$$K = \frac{S_n^*(d_S^*)^{\frac{w-1}{2-w}}}{q^*} \tag{16}$$

In the refined criteria equation, a dimensionless viscosity simplex μ^* was introduced, defined as:

$$\mu^* = \frac{\mu}{\mu_o} \tag{17}$$

Here $\mu_o = 0.059636$ Pa.s is the viscosity of standard hydraulic oil MHL 68 at temperature $T = 40$ °C.

The dynamic viscosity itself μ is defined through the kinematic viscosity ν and density ρ by the relationship:

$$\mu = \rho \cdot \nu \tag{18}$$

The dependence of viscosity and density on temperature was approximated, respectively, as:

$$\nu = -0.0038914 \cdot T^3 + 0.55695 \cdot T^2 - 28.7511 \cdot T + 571.583,\ \mathrm{mm^2/s} \tag{19}$$

$$\rho = 0.018782 \cdot T^2 - 2.0441 \cdot T + 905.03,\ kg/\mathrm{m^3} \tag{20}$$

Finally, the refined criteria equation for the volumetric efficiency η_v, valid for the considered design and operating modes, was derived as:

$$\eta_v = 1 - 1.3157569 \cdot 10^{-4} \mu^* \left(\frac{\pi_1}{\pi_2^{1.27}}\right)^{\frac{1}{0.73}} K, \tag{21}$$

and represents one of the objective functions subject to optimization.

2.4. Equation of the Actual Flow Rate (Second Objective Function)

For the optimization of the actual volumetric flow rate and the volumetric efficiency, taking the theoretical flow rate of the pump as

$$Q_t = q \cdot n, \tag{22}$$

the actual flow rate Q is defined by incorporating the volumetric efficiency η_v, which accounts for the internal losses:

$$Q = Q_t \cdot \eta_v \tag{23}$$

Equation (23) represents the second objective function subject to optimization.

3. Results and Discussion

Building entirely upon the theoretical and experimental apparatus summarized in Section 2, the present section presents the sequential implementation of the adopted research strategy. Since the mathematical models developed and validated in Part I describe a complex multiparametric system, the direct search for an optimal configuration is practically impossible. Therefore, the presentation follows the logic of constructive step-by-step development: it begins with an isolated numerical investigation of the individual geometric factors, proceeds through a rigorous analytical proof of their absolute optima, and concludes with the application of multicriteria optimization to resolve the identified engineering conflicts. This approach ensures that the final design recommendations are based on a stable and proven theoretical foundation.

3.1. Numerical and Analytical Investigation of the Influence of Gear Parameters on the Volumetric Efficiency and Actual Flow Rate of the Pump

It is well known from the theory of positive displacement hydraulic machines that volumetric losses are primarily determined by internal working fluid leakages through the radial and axial (face) clearances [42,43]. According to classical hydrodynamic

https://doi.org/10.3390/machines14070720

principles and Poiseuille's law for laminar flow in narrow gaps [44–46], the flow rate of these leakages is directly proportional to the operating pressure of the pump p and the cross-sectional area of the flow (clearances), while being inversely proportional to the dynamic viscosity μ of the fluid. Therefore, the influence of the main operating parameters on the volumetric efficiency η_v is physically justified and well documented in contemporary scientific literature.

Increased leakages directly generate larger volumetric losses, which leads to a significant reduction in the volumetric efficiency of the pump. In fact, according to Poiseuille's law [45], the flow through such gaps is directly proportional even to the cube of the clearance thickness, which makes these geometric dimensions critical for volumetric efficiency.

Although the overall physical picture of hydraulic losses is clear, for the considered innovative design of a three-rotor pump with bilateral lantern meshing, the isolated and combined influence of the specific geometric parameters on these leakages is not yet fully understood.

To investigate this problem, a detailed numerical and analytical analysis of the influence of geometry on the volumetric efficiency of the machine under various operating conditions and different viscosity values is conducted in this section. The study is based on the previously derived mathematical models—Equation (10) for determining the theoretical displacement volume and the refined criteria Equation (21) for the volumetric efficiency. Since a generalized geometric coefficient, combining all key dimensions of the gear meshing, is integrated into the structure of Equation (21), this model provides the necessary mathematical framework for a precise quantitative evaluation of the relationship between the pump geometry and its volumetric characteristics.

To ensure a correct comparative analysis of the pump's performance and efficiency in terms of flow rate, similar to the analysis of the displacement volume, strict constraints are imposed on the outer dimensions of the pump element. In the radial and axial directions, the root circle diameter of the hypocycloid gear d_{Hf} and the face width b are, respectively, assumed to be constant. According to the adopted methodology, with each variation in the independent parameters (z, r_c^*, or λ), the scale module of the gear m is recalculated relative to the fixed dimension d_{Hf} using Formula (4). Here, the relative clearances must be additionally recalculated using Equations (1) and (2). Otherwise, the flow cross-sections and the equivalent leakage clearances would change, which would compromise the objectivity of the comparison.

Based on this, a parametric study is implemented, in which the influence of the leading geometric factors—z,r_c^*, and λ—is sequentially isolated and analyzed. Within the scope of this study, we aim to answer the following questions:

- How do the dimensionless geometric parameters—the number of teeth z, the relative lantern radius r_c^*, and the cycloid shortening coefficient λ—affect the volumetric efficiency η_v, and at what values of these parameters is the maximum volumetric efficiency achieved?
- Is the maximum volumetric efficiency η_v realized with the same geometric parameters under all operating conditions and working fluid properties?
- Do the optimal geometric parameters of the pump coincide with respect to the criteria for maximum actual flow rate Q and maximum volumetric efficiency η_v?

3.1.1. Numerical Investigation of the Volumetric Efficiency

Using the refined Equation (21) for the volumetric efficiency, an analysis of the influence of the number of teeth z and the gear coefficients r_c^* and λ on the volumetric efficiency of the pump can be performed.

Figure 1 shows the dependence of the volumetric efficiency η_v on the relative lantern radius r_c^* and the cycloid shortening coefficient λ. To specifically isolate the influence of the coefficients that define the profiles of the cycloidal teeth, the remaining parameters are fixed. The values of the geometric quantities correspond to those of the physical prototype, namely: number of teeth $z = 7$, root circle diameter of the hypocycloid gear $d_{Hf} = 57$ mm, face width $b = 10$ mm, equivalent clearances $\delta_1 = \delta_2 = 0.012$ mm. With respect to the operating conditions and the properties of the fluid, in order to ensure the representativeness of the analysis, typical mean values are adopted: pressure $p = 20$ bar, rotational speed $n = 2000\ \text{min}^{-1}$, and viscosity $\mu = 0.05449$ Pa.s.

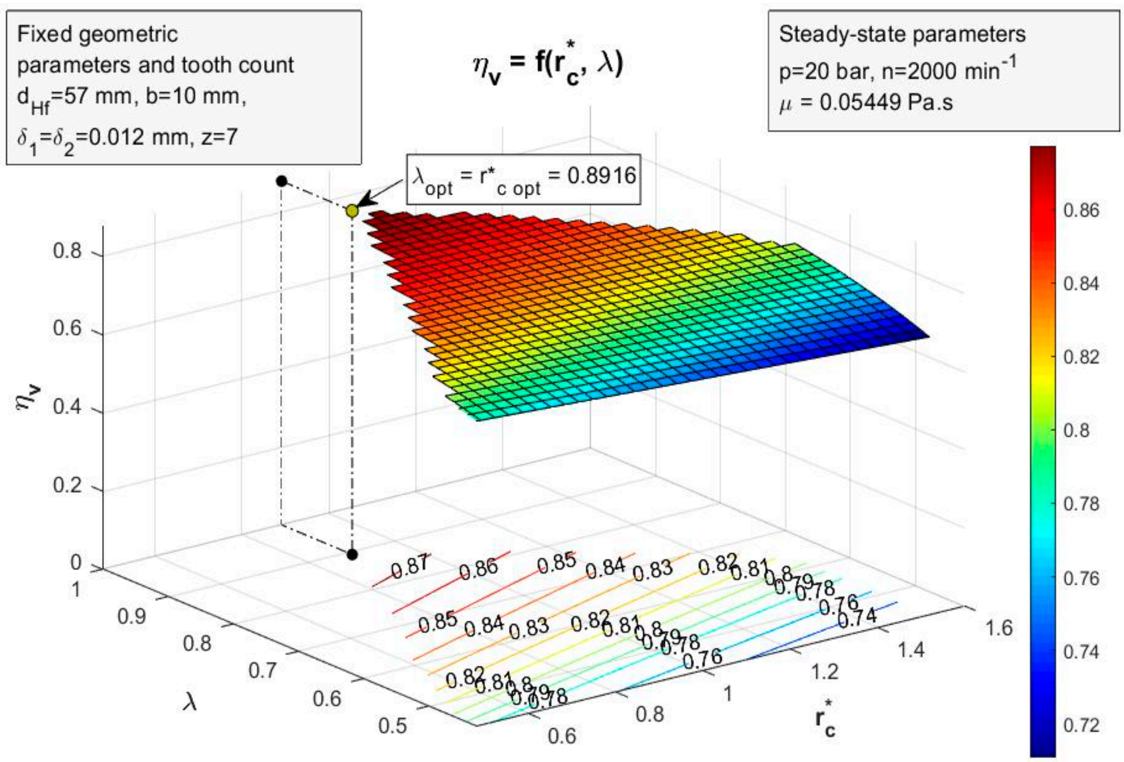

Figure 1. Dependence of the volumetric efficiency η_v on the relative lantern radius r_c^* and the cycloid shortening coefficient λ at the following constant values: number of teeth z, root circle diameter of the hypocycloid gear d_{Hf}, face width b, equivalent clearances δ_1 andδ_2, pressure p, rotational speed n.

It is evident that with a decrease in r_c^* and an increase in λ, the volumetric efficiency η_v increases relatively linearly, with the coefficient λ having a greater influence on the variation in the volumetric efficiency. In the entire range of $r_c^* = 0.4 \div 1.5$, the volumetric efficiency decreases by approximately 6% ($\eta_v \approx 78 \div 72\%$), while for $\lambda = 0.42 \div 0.89$ the increase is about 15% ($\eta_v \approx 76 \div 89\%$). The decrease in η_v with the increase in r_c^* is explained by the fact that as the radius of the lanterns increases, the area of the axial clearance between the lanterns and the lateral distributor, as well as the volumetric leakages through it (Figure 2), increase to a greater extent than the increase in the displacement volume q and the theoretical flow rate Q_T. The increase in the volumetric efficiency with the increase in λ is due to the fact that the displacement volume q and the theoretical flow rateQ_T become larger without significantly changing the radial clearance and the leakages Δq_1 within it (Figure 1 in [10]).

This also explains the more significant influence of λ on η_v compared with r_c^*, since with an increase in λ, the volumetric losses Δq_{22} in the axial clearance between the lanterns and the lateral distributor remain almost unchanged, unlike with the variation in r_c^*.

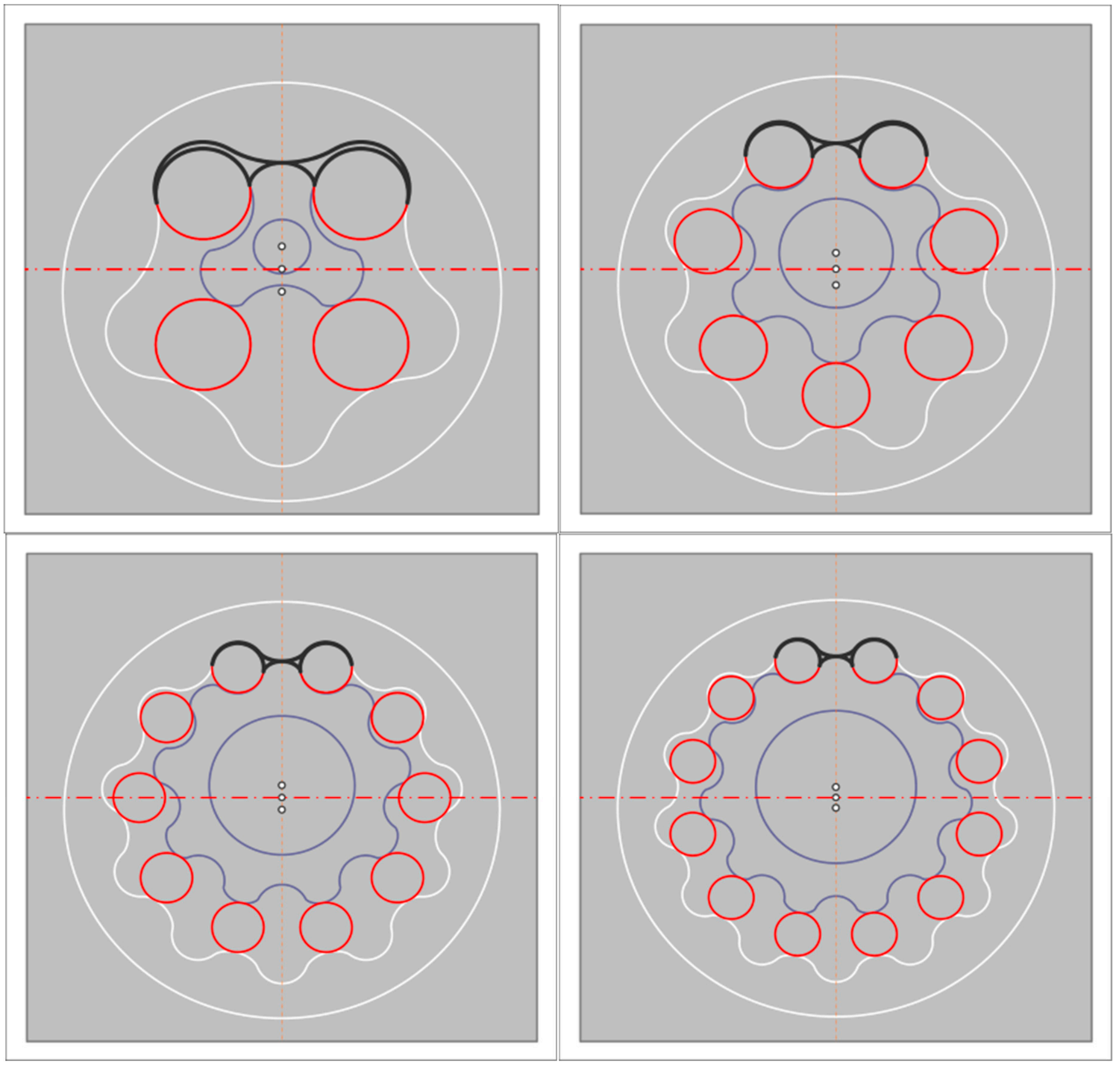

Figure 2. General view of the gear meshing geometry at a different number of teeth z and constant overall dimensions d_{Hf}.

From the above, considering the blocking contours of the gear (Figure 3 in [10]), it becomes clear that the volumetric efficiency also reaches its highest values at $r^*_{c,opt} = \lambda_{opt}$, as was also established for the displacement volume (see Equation (5)). Taking into account the complex influence of r^*_c and λ on the theoretical flow rate Q_T (displacement volume) and the volumetric efficiency, the pump will have the maximum actual flow rate Q again at $r^*_{c,opt} = \lambda_{opt}$.

Figure 3 shows the influence of the number of teeth z on the volumetric efficiency η_v at the same constant values: d_{Hf},$\delta_1 = \delta_2$, b, and μ.

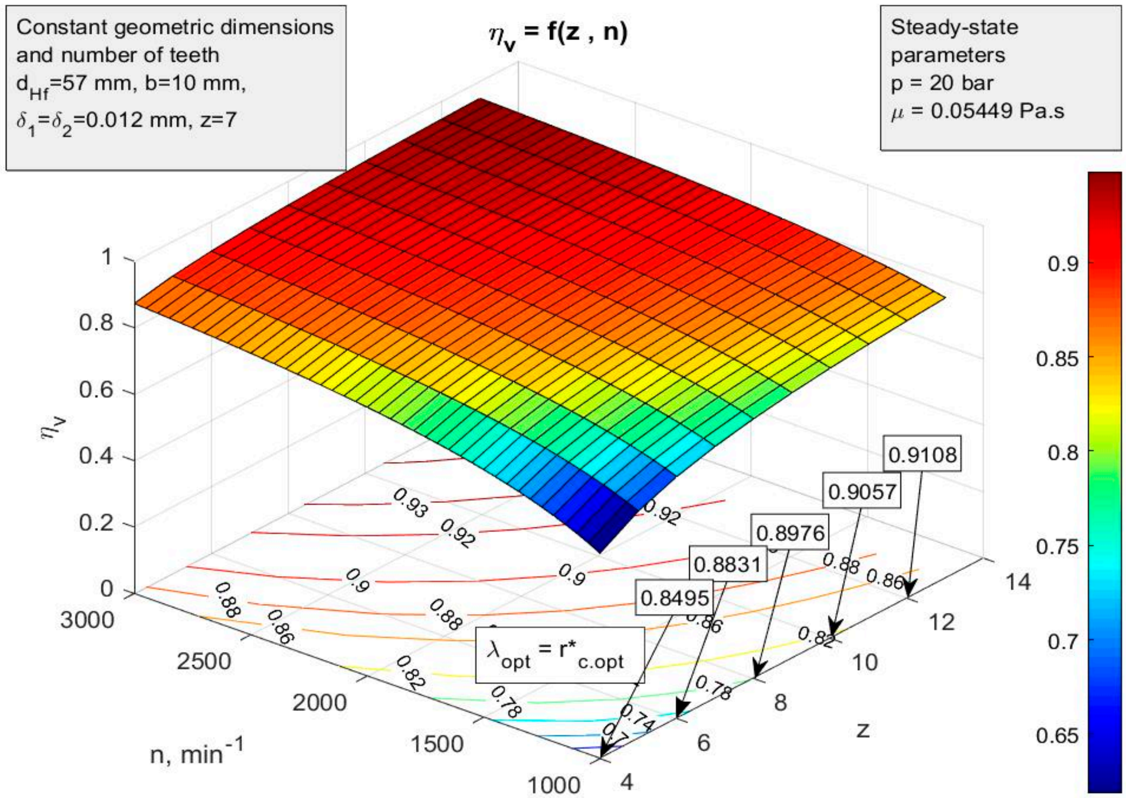

(**a**)

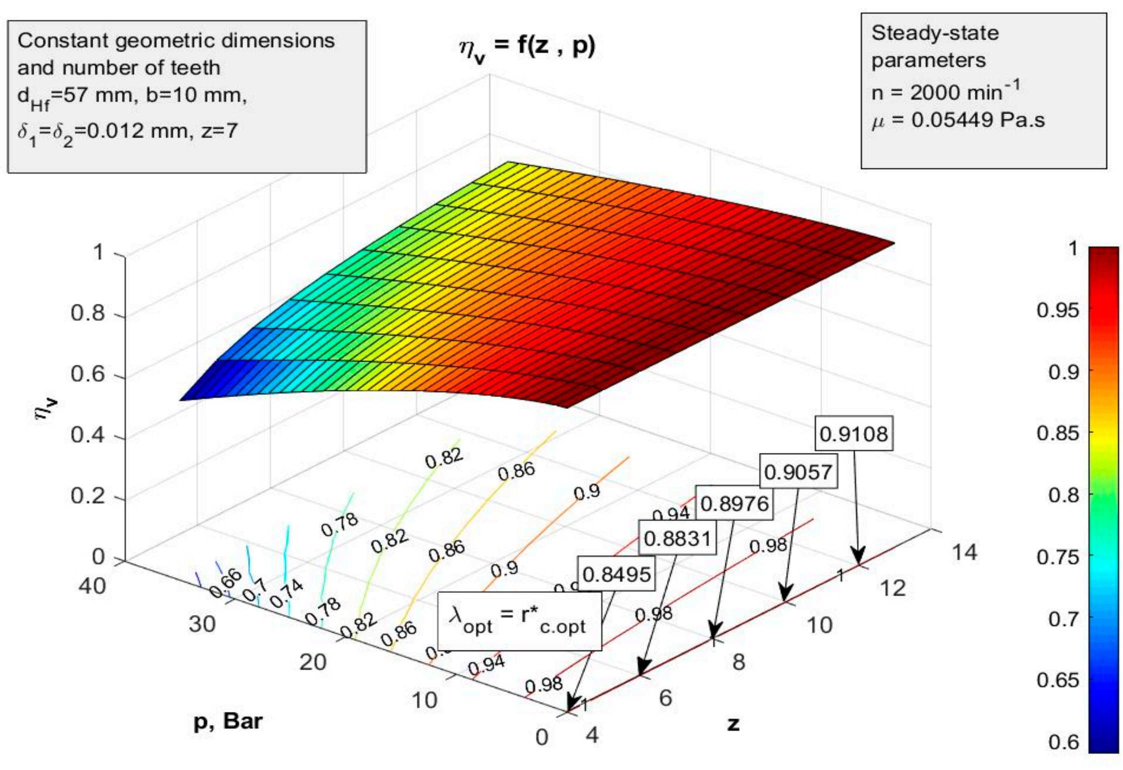

(**b**)

Figure 3. Dependence of the volumetric efficiency η_v on the number of teeth z, rotational speed n, and pump pressure p at the following constant values: root circle diameter of the hypocycloid gear d_{Hf}, face width b, equivalent clearances δ_1 and δ_2: (**a**) at constant pressure $p = 20$ bar; (**b**) at constant rotational speed $n = 2000\ \text{min}^{-1}$.

With an increase in z at a constant pressure $p = 20$ bar (Figure 3a), the volumetric efficiency η_v increases nonlinearly with a growth rate $O(z^h)$ (Landau symbol) and degree $0 < h < 1$, and at lower values of n, this dependence is more pronounced (h is closer to 0). For a number of teeth $z = 4 \div 13$ (a range whose lower boundary is determined by the unacceptable deterioration of the operating characteristics at a smaller number of teeth—mainly high flow-rate pulsation and problems with the sealing of the working chambers [5], while the upper boundary covers the most common design solutions) and a speed $n = 3000\ \text{min}^{-1}$, the volumetric efficiency increases by about 7% ($\eta_v \approx 88 \div 95\%$), whereas at $n = 1000\ \text{min}^{-1}$ this variation is within 19% ($\eta_v \approx 66 \div 85\%$). The considered boundary values of the rotational speed correspond to the experimentally established operating range of the investigated machine.

The increase in η_v with the increase in z at constant dimensions d_{Hf} and b can be explained by the fact that the radius of the lanterns decreases, which in turn reduces the displacement volume q and the volumetric leakages Δq_{22} in the axial clearance between the lanterns and the lateral distributor. However, the change in the leakages Δq_{22} is greater than the change in q, whereby the relative leakages $\Delta q_{22}/Q_T$ in this axial clearance decrease, and the volumetric efficiency η_v increases. The nonlinearity of this dependence is mainly due to the nonlinear variation in the lantern radius and the leakages Δq_{22}.

In all cases, low rotational speeds are unfavorable for the volumetric efficiency. For example, for $z = 6$, the volumetric efficiency is $\eta_v \approx 89\%$ at $n = 3000\ \text{min}^{-1}$ and $\eta_v \approx 74\%$ at $n = 1000\ \text{min}^{-1}$. This is explained by the decrease in the theoretical flow rate Q_T due to the reduction in the speed n and the insignificant change in the volumetric losses ΔQ. The increase in η_v with the increase in n is also nonlinear, with a growth rate $O(z^h)$ and degree $0 < h < 1$, being more pronounced for a smaller number of teeth z.

Figure 3b graphically presents the dependence of the volumetric efficiency η_v on the number of teeth z and the pressure p at a constant rotational speed $n = 2000\ \text{min}^{-1}$. It is known that as p increases, the volumetric efficiency η_v decreases due to the increased pressure drop in the flow passages of the machine. These results confirm the fundamental dependencies well known in the classical theory of positive-displacement gear machines [5]. The significance of this analysis lies in the quantitative assessment of this classical conflict (between the decreasing flow rate and the increasing volumetric efficiency) for the specific kinematics of the new three-rotor pump, which also creates the objective need for subsequent multicriteria Pareto optimization.

3.1.2. Comparative Analysis and Analytical Proof of the Global Optimum Regarding the Actual Flow Rate and Volumetric Efficiency

Since the actual flow rate depends on both quantities, the influence of z on the actual flow rate and how it quantitatively compares with the volumetric efficiency in quantitative terms are of particular interest.

Figure 4 graphically shows the variation in the actual flow rate Q and the volumetric efficiency η_v with a change in the number of teeth z, at optimal coefficients $r^*_{c,opt}$ and λ_{opt}, again constant dimensions $d_{Hf} = 57$ mm and $b = 10$ mm, clearances $\delta_1 = \delta_2 = 0.012$ mm, and average viscosity $\mu = 0.05449$ Pa·s. From the pressure isolines at an average constant rotational speed $n = 2000\ \text{min}^{-1}$ in $Q - z$ coordinates (Figure 4a), it can be seen that the pump has a maximum flow rate Q_{max} at $z = 5 \div 7$, with the influence of the number of teeth on the flow rate being more significant at lower pressures. For example, at the lower boundary of the investigated operating pressure $p = 5$ bar and $z = 4 \div 14$ (the already defined operating range), the flow rate Q varies by about 9 L/min (34% of Q_{max}), while at the maximum pressure for the same range $p = 35$ bar, this variation is about 3.7 L/min (19.5% of Q_{max}).

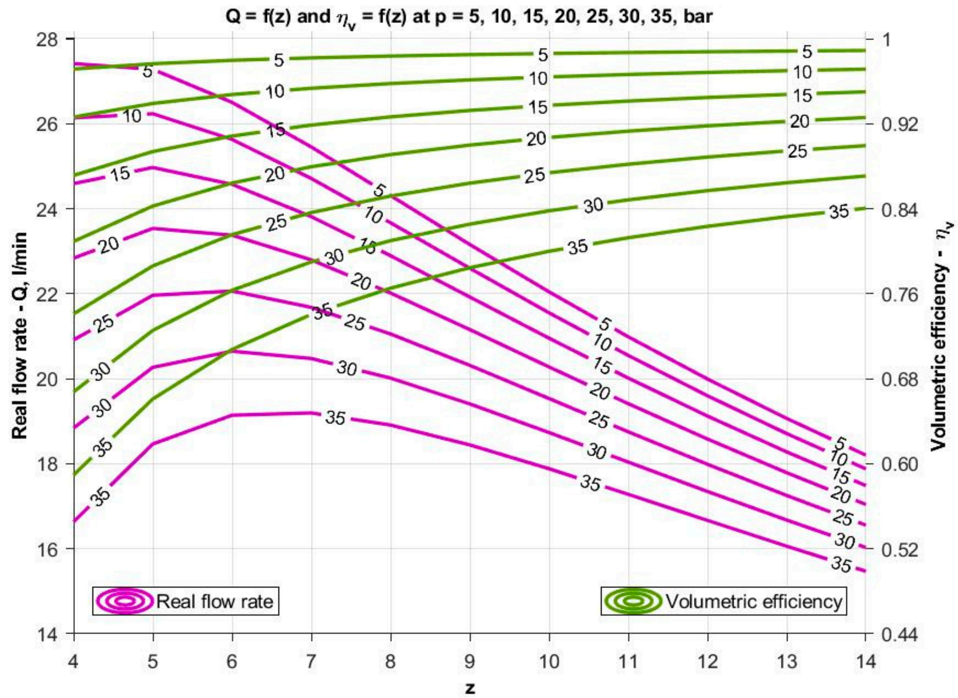

(**a**)

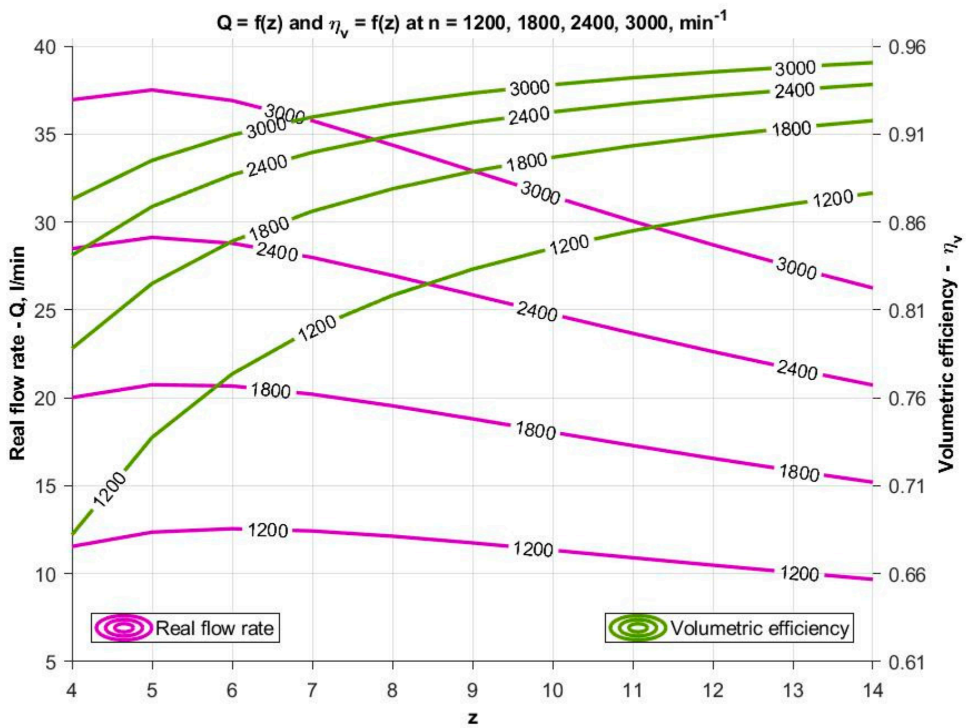

(**b**)

Figure 4. Dependences of the actual flow rate Q and the volumetric efficiency η_v on the number of teeth z at optimal coefficients $r^*_{c,opt}$ and λ_{opt}, constant dimensions $d_{Hf} = 57$ mm and $b = 10$ mm, clearances $\delta_1 = \delta_2 = 0.012$ mm, and viscosity $\mu = 0.05449$ Pa.s: (**a**) at various pressures p and a

constant rotational speed $n = 2000\ \text{min}^{-1}$; (**b**) at various rotational speeds n and a constant pressure $p = 20$ bar.

Considering the positive influence of z on the volumetric efficiency (Figure 4a), it is recommended in the design of pumps of this type that the number of teeth be selected between $z = 7 \div 10$. Larger values of z are recommended at higher pressures $p = 30 \div 35$ bar, and conversely, smaller values are preferred at lower pressures. In this way, a higher flow rate Q will be achieved without significantly affecting the effective operation of the pump (especially at rotational speeds $n = 2500 \div 3000\ \text{min}^{-1}$). At nominal operating modes ($p \approx 25$ bar), the volumetric efficiency η_v will decrease by approximately 5%.

The situation is analogous regarding the influence of z on the actual flow rate Q at different rotational speeds n and a constant pressure $p = 20$ bar (Figure 4b), although here this influence is more pronounced at higher rotational speeds. For example, at $n = 3000\ \text{min}^{-1}$ and $z = 4 \div 14$, the flow rate Q varies by about 10.5 L/min (28% of Q_{max}), while at $n = 1200\ \text{min}^{-1}$, this variation is about 6 L/min (40% of Q_{max}).

3.1.3. Conclusions and Formulation of a General Optimization Problem

The analysis of the numerical investigation conducted so far and the presented graphical dependences (derived for $z = 7$) reveals a clear trend: both in terms of the volumetric efficiency η_v and in terms of the displacement volume q and the theoretical flow rate Q_T, the maximums are reached at the exact same values of the relative lantern radius coefficient and the cycloid shortening coefficient—namely, at $r^*_{c,opt}$ and λ_{opt}. This provides strong grounds to hypothesize that this pattern is valid across the entire range of variation for the number of teeth z. Although this assumption could be verified by repeatedly performing numerical simulations for all possible values of z, it is much more rational and scientifically rigorous to prove the universality of these optimums strictly analytically.

Simultaneously, the numerical results also indicate a clear contradiction regarding the number of teeth z—a small number of teeth maximizes the flow rate, while a large number of teeth maximizes the volumetric efficiency. To provide a definitive answer to the raised questions, it is necessary to verify the following:

- Whether the established optimal values $r^*_{c,opt}$ and λ_{opt} remain valid under all possible operating modes (arbitrary pressures and rotational speeds).
- Whether these optimums are absolutely valid for any possible number of teeth z.
- Whether the conflicting trend in selecting the number of teeth z (maximum flow rate versus maximum volumetric efficiency) is preserved under all operating conditions and modes.

All of this can be proven through a single, comprehensive analytical proof. By formulating and solving a general optimization problem for the simultaneous maximization of the actual volumetric flow rate Q and the volumetric efficiency η_v, the universality of these patterns will be mathematically confirmed. This proof will guarantee that the established optimums are absolute, providing a solid foundation for the subsequent resolution of the conflict in selecting the optimal number of teeth z.

3.1.4. Definition of the Optimization Problem and Analytical Proof for the Global Optima

Based on the conclusions from the previous section, an analytical optimization problem is formulated and solved here to prove the existence of a global maximum of the considered objective functions for some fixed design and geometric parameters of the pump. In the present study, the term "global optimum" is used in a limited mathematical sense and refers to the two objective functions considered separately: the actual flow rate Q and the volumetric efficiency η_v. In this analytical step, the variables are λ, r_c^*, p, n, and T, while z, d_{Hf}, δ_1 and δ_2 are considered as fixed parameters. The aim is to show that the optimal values of λ, r_c^*, p, n, and T obtained in the separate optimization of Q and η_v coincide and remain valid for each fixed number of teeth z. The number of teeth z is then varied and considered as a discrete variable. At this stage, the problem is strictly bi-objective, since the two criteria conflict with respect to z: a smaller z favors the actual flow rate, whereas a larger z favors the volumetric efficiency. Therefore, a Pareto front is constructed, and one compromise solution is selected by means of the PSIMS method. Finally, in order to support practical design, an approximation formula is proposed for selecting z as a function of p and n.

The investigation is conducted using the already adopted fixed overall parameters $d_{Hf} = 57$ mm, $b = 10$ mm, and clearances $\delta_1 = \delta_2 = 0.012$ mm. This means that based on what has been stated so far, the vector X consists of the variables: $z, \lambda, r_c^*, p, \rho, n,$, i.e., $X = (z, \lambda, r_c^*, p, \rho, n, \mu)$.

As mentioned (Part I) in Formulas (19) and (20), based on experimental data, empirical relationships for the density ρ, kinematic and dynamic viscosity ν,μ as functions of temperature T were derived from experimental data. Thus, the investigated functions implicitly depend on the temperature T, and the vector X takes the form $X = X(z, \lambda, r_c^*, p, \rho, n, \mu, T)$.

Taking into account the objective functions (21) and (23) and constraint inequalities (6)–(10) and (26)–(42), the following bi-objective optimization problem and system of constraints are formulated:

$$\max\{Q(X)\} \tag{24}$$

$$\max\{\eta_v(X)\} \tag{25}$$

subject to constraints:

$$g_1(\lambda, r_c^*) = \lambda - \left(1 - \frac{4(z+1)^3 (r_c^*)^2}{27(z-1)z^2}\right)^{\frac{1}{2}} \le 0 \tag{26}$$

$$g_2(\lambda, r_c^*) = \lambda - r_c^* \le 0 \tag{27}$$

$$g_3(r_c^*) = r_c^* - \left(\frac{z}{2}\right)\sin\left(\frac{\pi}{z}\right) \le 0 \tag{28}$$

$$g_4(\lambda) = -\lambda + \frac{0.5}{\cos\left(\frac{1.15\pi}{z}\right)} \le 0 \tag{29}$$

$$h_1(\rho, T) = \rho - \rho(T) = 0 \tag{30}$$

$$h_2(\mu, \rho, T) = \mu - \rho(T)\nu(T) = 0 \tag{31}$$

$$z \le 17 \tag{32}$$

$$z \ge 4 \tag{33}$$

$$r_c^* \le 1.6 \tag{34}$$

$$r_c^* \ge 0.5 \tag{35}$$

$$p \le 55 \tag{36}$$

$$p \ge 5 \tag{37}$$

$$T \leq 50 \tag{38}$$

$$T \geq 25 \tag{39}$$

$$n \geq 1000 \tag{40}$$

$$n \leq 3600 \tag{41}$$

$$z \in Z; \quad \lambda, r_c^*, p, \rho, n, \mu, T \in R^+ \tag{42}$$

The problem (24)–(42) formulated in this way is a multi-objective mixed-integer nonlinear optimization problem. The multi-objective nonlinear problem with mixed-integer variables (MOMINLP type) is mainly characterized by the fact that instead of a single "best" answer, there is usually a set of non-dominated (Pareto-optimal) solutions, among which a subsequent choice is made according to preferences or a selection rule [33,34]. The nonlinearity almost always introduces nonconvexity and multiple local optimums, so the front might be discontinuous, disconnected, or nonconvex, and methods such as linear combination with weights often capture only a part of it. The integer variables add discreteness and lead to clusters of solutions and jumps in the front, because when changing an integer value, the structure of the feasible set and the optimal compromises change sharply [35–37]. This makes the solution sensitive to starting points, scaling/normalization of the criteria, and the method of constraint handling, as well as requires reliable MINLP strategies [36–38]. Therefore, in real-world applications, hybrid strategies are often used—for example, looping over the integer values and solving a continuous subproblem, after which the non-dominated ones are filtered and a selection criterion is applied. Alternatively, population-based heuristics/metaheuristics (e.g., MOEA/NSGA-II) are also used, which are convenient for approximating complex, nonconvex fronts with limited analytical information [39,40].

The specific nature of the model and the dimensionless groups used suggest that the two criteria do not enter into a significant conflict over a wide range of feasible modes, but rather vary in tandem: conditions that increase the energy and hydrodynamic "capacity" of the system simultaneously support both the increase in flow rate and the preservation/increase in efficiency. From a physical point of view, this leads to the hypothesis that the optimal modes are realized at the boundaries of the feasible domain for some of the controllable parameters, namely at minimum temperature, minimum pressure, and maximum rotational speed, which is typical for problems with pronounced monotonic relationships [41].

This hypothesis serves as the motivation for an analytical approach, in which, relying on the monotonic properties of the objective functions and the constraint conditions, a strict justification is sought that the indicated boundary modes are indeed optimal (or Pareto-optimal) for the considered model and constraints.

As previously established, the maximum displacement volume is obtained at point T_{opt} within the domain of existence of the gear at λ_{opt} and $r_{c,opt}^*$ (given in Equation (5)). This motivates checking whether the optimal solution for both criteria (24, 25) is located at the same point and conditions:

$$T = T_{min}; \quad p = p_{min}; \quad n = n_{max}.$$

The proof of the above statement is given in Appendix A.

In summary, the general mathematical proof conducted fulfills its main purpose—to strictly validate the engineering hypotheses proposed based on the numerical investigation. The connection between the proposed hypotheses and the analytical proofs can be systematized as follows:

- **Regarding the influence of operating modes:** Through Stage I (Lemma 1), the strict global monotonicity of the objective functions with respect to the pressure p, the rotational speed n, and the temperature T is proven. This definitively confirms the hypothesis that the geometric optima remain valid under all possible operating modes.
- **Regarding the universality at an arbitrary number of teeth** z**:** Through Stage II (Lemma 2 and Lemma 3) and the subsequent Theorem 1 and Theorem 2, it is proven that for any fixed $z \in \{4, \dots, 17\}$, the extrema of the two objective functions (24)–(25), taken separately, always lie on the boundary of the feasible set defined by the expressions for $r^*_{c,opt}$ and λ_{opt}. This proves that the optimal geometry of the profile does not depend on the number of teeth.
- **Theorem 3** proves that the two criteria (flow rate and volumetric efficiency) reach their global maximum at the same point with respect to the continuous geometric parameters.
- **Regarding the discrete parameter** z, a conflict is observed between the two criteria under all operating regimes.

The conducted analytical proofs provide a definitive answer to the raised questions: the optimal values of $r^*_{c,opt}$ and λ_{opt} remain valid and unchanged under all possible operating modes, as well as at an arbitrarily selected number of teeth z. However, with respect to the selection of the number of teeth z itself, the conflict between the actual flow rate Q and the volumetric efficiency η_v remains valid under all operating regimes. For the compromise resolution of this contradiction, multicriteria Pareto optimization can be applied, which is the subject of investigation in the next subsection.

3.2. Multi-Objective Pareto Optimization and Selection of the Optimal Number of Teeth Under Various Operating Modes

Based on the conclusions from the previous section and the conducted analytical proofs (Appendix A), the geometric parameters $r^*_{c,opt}$ and λ_{opt} have already been defined as constant global optima for the system under all operating conditions. However, the question of selecting the number of teeth z remains unresolved. Since, with respect to this discrete variable, it has been proven that an unavoidable engineering conflict exists between the two objective criteria—the maximization of the flow rate Q and the volumetric efficiency η_v—their simultaneous satisfaction represents a problem from the class of mixed-integer nonlinear programming (MINLP).

As justified in the literature review, classical gradient-based or stochastic methods cannot independently resolve such a multi-objective contradiction involving discrete variables without imposing preliminary subjectivity, for example, by using weighting coefficients. Therefore, in order to overcome this conflict, multicriteria Pareto optimization is applied in the present subsection. This mathematical apparatus enables the simultaneous and equivalent consideration of the two objective functions, deriving a set of nondominated solutions (Pareto fronts), which serves as an objective basis for subsequent engineering selection.

To ensure clarity and logical progression, the study follows a strictly defined logical sequence, including the following main stages:

- **Discretization of the operating space:** Defining a two-dimensional grid of operating modes (varying pressures p and rotational speeds n).
- **Generation and ranking of solutions:** For each individual mode, the bi-objective problem is solved, generating non-dominated solutions (Pareto fronts). By applying a specialized ranking method, a single, most balanced compromise optimum for the corresponding mode is objectively selected.

- **Analysis of physical trends:** Investigating the obtained optimal values for the number of teeth z and providing a physical explanation of the patterns governing them as the operating pressure and rotational speed change.
- **Derivation of an engineering mathematical model:** As a final and practically most significant result, the array of optimal solutions will be approximated. An algebraic relationship is derived, which allows the direct calculation of the optimal number of teeth as a function of the specified operating parameters and modes.

3.2.1. Multi-Objective Pareto Optimization

According to the formulated logical sequence, the study begins with the first stage—discretization of the operating space. For this purpose, a two-dimensional parametric sweep is implemented over a discrete grid of operating points (p, n), where the pressure varies as $p = 5 \cdot k$ bar (for $k = 1, \ldots, 11$), and the rotational speed as $n = 500 \cdot k$ min^{-1} (for $k = 2, \ldots, 7$). When generating these points, the geometric coefficients are assumed to be uniquely defined by the already proven Equation (A20) for $r^{*}_{c,opt}$ and λ_{opt}.

For each combination of pressure and rotational speed, the bi-objective optimization problem is solved. Each solution represents a collection of Pareto-optimal points [47]. A specific number of teeth z corresponds to each non-dominated point. These points are ranked using the PSIMS (Parameter Space Investigation with μ-Selection) method [48,49]. This approach reduces the Pareto front to ranked subsets, with the point having the maximum rank being selected as the Salukvadze optimum [50]—the solution that most uniformly approximates the utopian values under the hypothesis of equivalent criteria.

3.2.2. Selection of the Optimal Number of Teeth Under Various Operating Modes

Each optimal point generates a two-dimensional grid of "optimal" number of teeth for a specific (p, n) combination, presented in Figure 5.

Consistent trends are observed. For a fixed rotational speed n, the number of teeth z increases with an increase in pressure p, and this trend intensifies at low speeds. Conversely, at a fixed pressure, the number of teeth decreases with an increase in speed. This functional dependence $z = f(p, n)$ can be approximated extremely accurately with a power law of the form:

$$f(p, n) = cp^{a}n^{b} + d \tag{43}$$

After approximating the experimental data, the parameter values (and their confidence intervals) are:

$$a = 1.158 \quad (0.9727,\ 1.344)$$

$$b = -0.838 \quad (-0.9454,\ -0.7306)$$

$$c = 24 \quad (8.134,\ 39.86)$$

$$d = 7.186 \quad (6.879,\ 7.493)$$

The approximation has a high coefficient of determination $R^2 = 0.9603$, which confirms its adequacy (Figure 6a). Since the number of teeth is a natural number, the model is rounded to:

$$f_r(p, n) = \mathrm{round}(cp^{a}n^{b} + d) \tag{44}$$

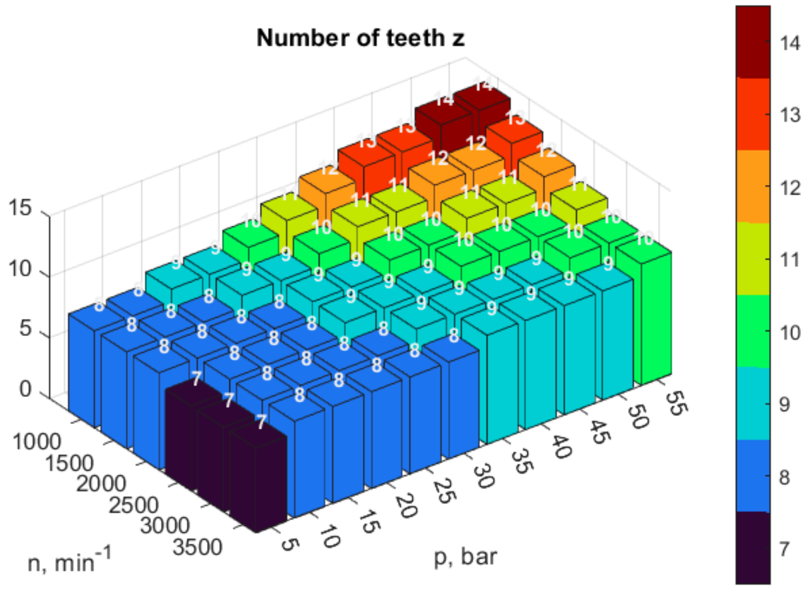

Figure 5. Optimal number of teeth z for a set of pressures p and rotational speeds n.

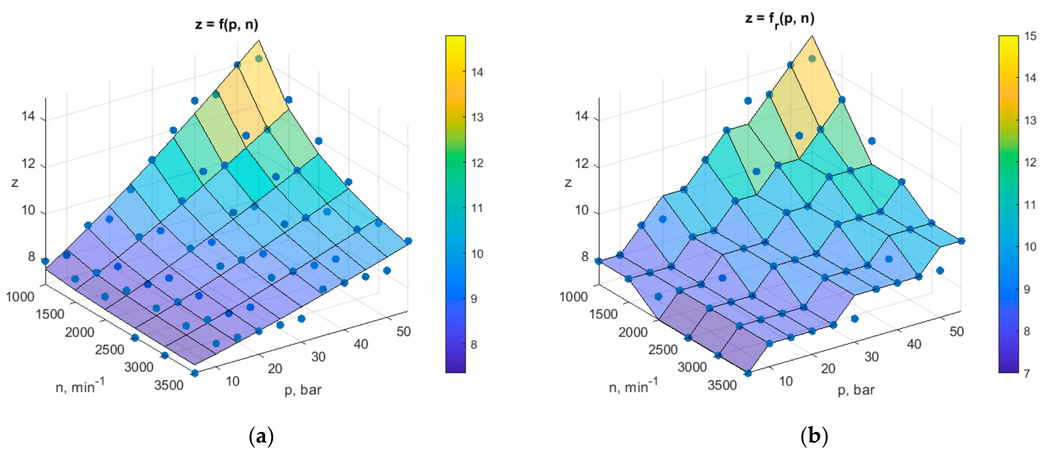

Figure 6. Optimal number of teeth z—experimental (points) and approximated (surface) values: (**a**) model according to Equation (43); (**b**) model with rounding to an integer (44).

These dependencies have a clear physical explanation. The actual flow rate and volumetric efficiency are related by:

$$Q = q \cdot n \cdot \eta_v \tag{45}$$

$$\eta_v = 1 - C \cdot K \cdot \pi_1^{\frac{1}{0.73}} \pi_2^{-\frac{1.27}{0.73}} \tag{46}$$

This yields the relationship for the losses:

$$\pi_1^{\frac{1}{0.73}} \pi_2^{-\frac{1.27}{0.73}} \sim p^{\frac{1}{0.73}} n^{-1} \tag{47}$$

Increasing the pressure p amplifies the leakages (the penalty term), which requires a geometry with higher hydraulic tightness (a larger number of teeth z). Conversely, as n increases, the relative influence of leakages weakens, allowing the selection of a smaller number of teeth, favoring the larger displacement volume q.

As seen from Figure 7, high values of volumetric efficiency ($\eta_v > 0.95$) are achieved primarily at low pressures. The derived patterns and Equation (43) provide a powerful and easy-to-use engineering tool for selecting the optimal number of teeth when

https://doi.org/10.3390/machines14070720

designing three-rotor pumps for specific operational conditions and operating modes. When searching for the optimal number of teeth z_{opt} under various operating modes, it is already definitively clear that the optimal values of the relative lantern radius and the cycloid shortening coefficient must be adopted according to the derived Equation (A20).

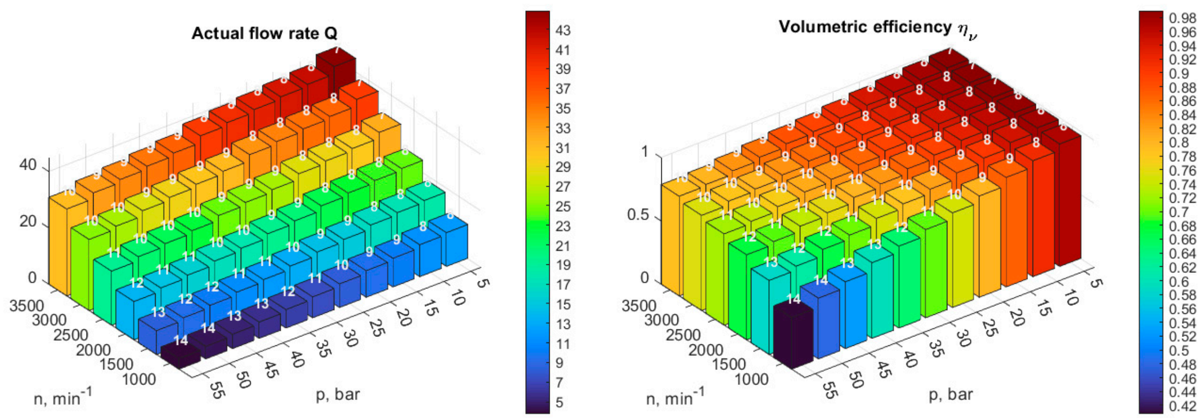

(**a**) (**b**)

Figure 7. Optimal number of teeth z (integers) and their corresponding characteristics for a set of p and n: (**a**) actual flow rate Q; (**b**) volumetric efficiency η_v.

The conducted parametric numerical investigation and the subsequent multicriteria optimization reveal the complex interrelationship between the geometric parameters and the operating performance indicators of the three-rotor pump with lantern meshing. The obtained results highlight several key discussion points, which have both theoretical and direct practical significance.

First, the analytical proof of the invariance of the optimal values of the relative lantern radius $r^*_{c,opt}$ and the cycloid shortening coefficient λ_{opt} represents a substantial contribution to the geometric theory of this type of machine. The fact that these coefficients ensure a global maximum simultaneously for the working displacement q, the actual flow rate Q, and the volumetric efficiency η_v, independently of the operating pressure p or the rotational speed n, significantly simplifies the selection of these parameters in the initial stages of design. This means that the designer can preliminarily fix these two parameters according to the established optima, eliminating them as variables in the subsequent optimization process.

Second, the results clearly define and quantitatively express the main engineering conflict with respect to the number of teeth z. It was established that decreasing the number of teeth leads to a significant increase in the specific working displacement, but at the same time shortens the length of the sealing clearances, which reduces the hydraulic sealing of the gearing and leads to a decrease in the volumetric efficiency η_v, especially at higher pressures. Conversely, a larger number of teeth improves the sealing, but limits the flow rate while preserving the same external dimensions. This analytically irresolvable conflict proves that there is no single "perfect" geometry for all cases, and that the optimum is strictly dependent on the specific application and operating regimes of the pump.

It is precisely here that the strength of the applied multicriteria Pareto optimization (MINLP) becomes evident. Through it, the problem is transferred from the sphere of theoretical compromises into the field of exact mathematical solutions. The generated Pareto fronts and their ranking by the PSIMS method allow an objective selection of configurations. The algebraic relationship $z_{\text{opt}} = f(p, n)$ derived as a result is a practical outcome of the study. With a very good coefficient of determination ($R^2 = 0.9603$), this empirical function transforms the complex optimization algorithm into an accessible algebraic engineering relationship.

The obtained optimal parameters have a direct engineering interpretation. First, the values of $r^*_{c,opt}$ and λ_{opt} fix the basic geometry of the lantern meshing. Then, for a given operating pressure p and rotational speed n, the derived approximation relationship allows the recommended number of teeth z to be selected. After the selection of z, r^*_c, and λ, the scale module m is determined from the specified external size d_{Hf}, and from it the real design dimensions of the pump element are obtained. Therefore, the proposed methodology may be used as a tool to support the initial stage of design. However, it does not replace the final engineering verification, in which the manufacturability of the cycloidal profiles and lanterns, the achievable clearances, the strength and stiffness of the elements, the bearing loads, the tribological conditions, the flow-rate pulsations, the risk of cavitation, and the acoustic characteristics must be taken into account.

In summary, the proposed methodology not only explains the physical behavior of three-rotor pumps with lantern meshing but also closes the cycle from pure mathematical modeling to direct industrial application, providing designers with a clear algorithm for creating highly efficient hydraulic machines with respect to performance and volumetric losses, adapted to specific operating regimes.

Regarding the "universality" of the profile optima ($r^*_{c,opt}$ and λ_{opt}): The claim of universality, stated in Part I and proven in Part II (Theorems A1, A2, and A3), refers strictly and solely to the geometric optima of the profile. As is evident from the mathematical proofs in Part II, the determination of the global extremum with respect to these two parameters is carried out by investigating the monotonicity of the generalized geometric coefficient K, the function $P(\lambda, r^*_c)$. These proofs arise from the structure of the geometric relationships themselves and do not depend on the numerical values of the empirical coefficients (B_1 and w). Therefore, although the model is calibrated on one prototype, the mathematical conclusion that these optima are valid for this type of cycloidal machine remains strictly analytically justified.

In this context, it is important to clarify that although the coefficients in the criterion equation for the volumetric efficiency are determined through experimental data obtained from one specific prototype, the analytical conclusions drawn are not limited solely to it. The experimental data mainly serve to calibrate the numerical values in the model, whereas the regularities concerning the location of the profile optima and the conflict between the actual flow rate and the volumetric efficiency with respect to the number of teeth z are derived from the geometric structure of the considered type of pump. In order to specify the scope of this validity, Theorem A4 is formulated in Appendix A, demonstrating that the proofs retain their validity for calibration coefficients within the limits $B_1 > 0$ and $1 < w < 1.30$. Therefore, insofar as the calibration coefficients remain within these proven limits, the conclusions drawn should be considered valid for this type of three-rotor pump with lantern meshing, and not only for the experimentally investigated prototype.

It is important to emphasize the strict scope of the conducted optimization. Since the considered three-rotor pump has an innovative kinematic structure, the construction of its mathematical apparatus follows a clear hierarchy, and the present study deliberately limits itself to maximizing the actual flow rate and the volumetric efficiency. Undoubtedly, a complete performance assessment requires additional analysis of torque, mechanical and overall efficiency, evaluation of mechanical and hydraulic losses, tribological investigations of wear, as well as analysis of acoustic indicators, etc. Nevertheless, their reliable mathematical modeling for this new design is practically impossible without a previously clarified and optimized volumetric-geometric basis. In this sense, the proposed methodology does not claim to provide an exhaustive multiphysical global optimum of the machine as a whole but defines its absolute volumetric optimum. This result has fully independent scientific and applied significance and provides the necessary fundamental basis for the subsequent development of models for mechanical and hydraulic losses.

4. Conclusions

Building upon the mathematical models validated in Part I and the numerical and analytical investigations conducted in this Part II, the following main conclusions are drawn:

- Through a parametric numerical investigation across the entire domain of existence of the gear, conducted at a fixed number of teeth, the optimal values of the dimensionless geometric parameters were established: the relative lantern radius $r_{c,opt}^{*}$ and the cycloid shortening coefficient λ_{opt}. These values, calculated using Formula (5), coincide with the optimums established in [51] for achieving maximum displacement volume. Since the actual flow rate is proportional to the displacement volume and the volumetric efficiency, it follows that it also reaches its maximum at the same coefficient values.
- The results of the numerical investigation at a specific operating mode indicate a conflict regarding the number of teeth z—a small number of teeth contributes to maximizing the displacement volume, while a large number of teeth leads to an increase in volumetric efficiency.
- The results of the numerical investigation demonstrate the need for a general proof valid for all modes, and in this regard, a rigorous analytical proof is presented, based on investigating the extremums of the criteria equation, confirming the universal nature of the established geometric optima. It is proven that $r_{c,opt}^{*}$ and λ_{opt} do not depend on the operating mode (pressure and rotational speed), fluid properties (viscosity), or the selected number of teeth z.
- A multi-objective Pareto optimization (MINLP) procedure was applied to maximize the actual flow rate and volumetric efficiency, successfully resolving the conflict between high displacement volume and hydraulic tightness. Pareto fronts are generated, which are ranked using PSIMS selection, objectively choosing the optimal values for the number of teeth z_{opt} for the specific operating mode—working pressure p and rotational speed n.
- A functional relationship$z_{opt} = f(p, n)$ was derived, approximating the results of the Pareto optimization with high accuracy ($R^2 = 0.9603$). This formula could be used as a tool to support the initial design stage, but strictly with respect to the volumetric performance indicators of the pump, namely the actual flow rate and the volumetric efficiency. However, it categorically does not replace the final engineering verification for the corresponding specific application.

In the future, it is planned to use the developed prototype as a component of an electro-hydraulic servo drive system. In this type of system, regardless of whether modified PID controllers [52] or model predictive control (MPC) algorithms [53] are applied, the availability of an adequate mathematical model of the flow rate and volumetric leakages is critical for the control quality. Therefore, the obtained empirical dependencies for the actual flow rate and volumetric efficiency of the current prototype will be integrated into the mathematical model of the future servo system. This is expected to contribute to a higher degree of agreement between the numerical simulations and the real experimental data under dynamic operating conditions. Analogous to the temperature compensation approach proposed in [54], the same dependencies will be utilized in simulating the servo system under variable temperature and operational conditions. Since the change in temperature directly affects the dynamic viscosity and density of the working fluid (which is already accounted for in the derived pump equations), this directly impacts the nature of the ongoing dynamic processes. The use of the proposed model, accounting for these influences, will create prerequisites for a better correlation between the numerical modeling of the processes and the actual system performance.

Another direction for the future development of the present study is the extension of the developed methodology to the investigation of the torque and mechanical efficiency. Based on the defined pump geometry and depending on the operating pressure, dependencies for the theoretical torque can be obtained. By applying the mathematical apparatus of similarity theory and dimensional analysis, the dimensionless similarity criteria governing the mechanical losses are to be identified. This will allow the formulation of a mathematical model in the form of a criterion equation for the mechanical efficiency, whose empirical coefficients will be refined using experimental data. The joint determination of the dependencies for the theoretical torque and mechanical efficiency will provide the necessary basis for investigating the actual pump torque, as well as for its optimization concerning the geometric parameters under various operating conditions.

Author Contributions: Conceptualization, I.N. and I.G.; methodology, I.N.; software, I.G. and S.G.; validation, I.N., I.G. and S.G.; formal analysis, I.N.; investigation, I.N. and I.G.; resources, I.N. and I.G.; data curation, I.N. and S.G.; writing—original draft preparation, I.N. and S.G.; writing—review and editing, I.N., I.G., S.G. and G.I.; visualization, S.G.; supervision, I.N.; project administration, I.N. and S.G.; funding acquisition, I.N., I.G. and S.G. All authors have read and agreed to the published version of the manuscript.

Funding: This study was financed by the European Union—NextGenerationEU, through the National Recovery and Resilience Plan of the Republic of Bulgaria, project No. BG-RRP-2.013-0001.

Data Availability Statement: Data is contained within the article.

Acknowledgments: The authors are grateful to the anonymous reviewers, whose constructive comments have significantly contributed to the improvement of the quality of the paper.

Conflicts of Interest: The authors declare no conflicts of interest. The funders had no role in the design of the study; in the collection, analyses, or interpretation of data; in the writing of the manuscript; or in the decision to publish the results.

Abbreviations

The following abbreviations are used in this manuscript:

MINLP	Mixed-Integer Nonlinear Programming
MOMINLP	Multi-Objective Mixed-Integer Nonlinear Programming
PSIMS	Parameter Space Investigation with μ-Selection
MOEA	Multi-Objective Evolutionary Algorithm
NSGA-II	Non-dominated Sorting Genetic Algorithm II
SI	International System of Units
MPC	Model Predictive Control
PID	Proportional-Integral-Derivative

Nomenclature

b	Gear width
b^*	Relative gear width
d_{Hf}	Root circle diameter of the hypocycloidal gear
d_s	Hydraulic diameter of the equivalent clearance
d_s^*	Dimensionless hydraulic diameter
Eu	Euler number for dimensionless pressure

$\vec{F}$ Force acting on the pin center
K Generalized dimensionless geometric coefficient
m Scale module of the gear
n Rotational speed
p Operating pressure (pressure drop)
Q Actual volumetric flow rate
Q_T Theoretical flow rate
q Volumetric displacement
q^* Dimensionless volumetric displacement
Δq_1 Leakages in the radial clearance
Δq_{22} Volumetric losses (leakages) in the axial clearance between the pins and the front distributor
Re Reynolds number for dimensionless viscosity
r_c^* Relative pin/lantern radius
$r_{c,opt}^*$ Optimal relative pin/lantern radius
r_{uc}^* Interference limit between adjacent pins
S_n Cross-sectional area of the total equivalent clearance
S_n^* Dimensionless cross-sectional area of the equivalent clearance
T Fluid temperature
$\vec{v}$ Velocity of the point of application
X Vector of variables
z Number of teeth (pins) of the central rotor
z_{opt} Optimal number of teeth

Greek Symbols

δ_1 Equivalent radial clearance
δ_2 Equivalent axial clearance
δ_1^* Relative equivalent radial clearance
δ_2^* Relative equivalent axial clearance
$\varepsilon_{u,min}$ Minimum contact ratio
η_v Volumetric efficiency
$[\theta]$ Permissible force transmission angle (pressure angle)
λ Shortening coefficient of the cycloids
λ_{opt} Optimal shortening coefficient of the cycloids
λ_{Emax} Undercutting limit of the epicycloidal teeth
λ_{max} Interference limit between the cycloidal teeth
μ Dynamic viscosity
μ_o Viscosity of standard hydraulic oil at 40 °C
μ^* Dimensionless viscosity simplex
ν Kinematic viscosity
π_1 Euler number (analytical similarity criterion for pressure)
π_2 Reynolds number (analytical similarity criterion for viscosity)
ρ Fluid density

Appendix A. Proof for "Global Optimality"

The proof will be conducted in several stages. First, an analytical proof for the single-objective problem $\max \eta_v$ at fixed geometric parameters and a fixed z, under the constraints for the feasible domain of solutions and the real domain $r_c^* \in [0.5,1.6]$. The proof is organized in two steps: Stage (I)—global monotonicity with respect to (p, n, T) and Stage (II)—reduction and global optimality with respect to (λ, r_c^*).

Before proceeding to the proof, the following notations are introduced for convenience:

$$u(\lambda, r_c^*, z) = \frac{1}{m} = \frac{z+\lambda+2r_c^*}{d_{Hf}} \tag{A1}$$

After converting the units according to the International System of Units (SI), the similarity criteria π_1 and π_2 take the form:

$$\pi_1 = p\frac{100{,}000}{\rho\left(n\frac{m}{60{,}000}\right)^2} \tag{A2}$$

$$\pi_2 = \frac{\mu}{\rho\left(\frac{n}{60}\right)\left(\frac{m}{1000}\right)^2} \tag{A3}$$

The multiplier $K(\lambda, r_c^*; z)$ rewritten in another form is:

$$K = \frac{N}{\left(\frac{b}{m}\right)z^{1.11}R^{\frac{1.27-1}{1.27-2}}(476\lambda - 11r_c^* + 10)} \tag{A4}$$

where:

$$N = 3\left(\frac{b}{m}\right)\left(\frac{\delta_1}{m}\right) + 4\left(\frac{\delta_2}{m}\right)r_c^* + \left(\frac{\delta_3}{m}\right)\pi(\lambda + 2r_c^* + z) \tag{A5}$$

$$R = \frac{12\left(\frac{b}{m}\right)\left(\frac{\delta_1}{m}\right) + 16\left(\frac{\delta_2}{m}\right)r_c^* + 4\left(\frac{\delta_3}{m}\right)\pi(\lambda + 2r_c^* + z)}{6\left(\frac{b}{m}\right) + 6\left(\frac{\delta_1}{m}\right) + 8\left(\frac{\delta_2}{m}\right) + 8r_c^* + 2\pi(\lambda + 2r_c^* + z)} \tag{A6}$$

The objective function of the volumetric efficiency is:

$$\eta_v = 1 - C_0\left(\frac{\mu}{\mu_0}\right)\left(\pi_1^{\frac{1}{0.73}}\pi_2^{-\frac{1.27}{0.73}}\right)K \tag{A7}$$

where $C_0 = 0.000131375275$, $\mu_0 = 0.05448964$. After substituting $\rho = \rho(T)$, $\mu = \mu(T) = \rho(T)\nu(T)$ and performing algebraic transformations, the objective function becomes:

$$\eta_v = 1 - Cp^{\frac{1}{0.73}}n^{-1}\rho(T)^{-\frac{0.27}{0.73}}\nu(T)^{-\frac{0.54}{0.73}}u(\lambda, r_c^*; z)^{\frac{0.54}{0.73}}K(\lambda, r_c^*; z), \tag{A8}$$

where $C > 0$ is a constant (independent of p, n, T, λ, r_c^*), and $u = \frac{1}{m}$.

Appendix A.1. Stage (I)—Global Monotonicity with Respect to (p, n, T)

Lemma A1. *(Global maximum with respect to* p, n, T*). For fixed* (λ, r_c^*)*, the function* η_v *is strictly decreasing with respect to* p*, strictly increasing with respect to* n*, and for* $T \in [25{,}50]$ *it is strictly decreasing with respect to* T*. Therefore, the global maximum with respect to* (p, n, T) *is reached at* $p = p_{min}$*,* $n = n_{max}$*,* $T = T_{min}$*.*

Proof. From (50), the negative term is proportional to $p^{\frac{1}{0.73}}$ (a positive power), to n^{-1}, and to $\rho(T)^{-\frac{0.27}{0.73}}\nu(T)^{-\frac{0.54}{0.73}}$. Thus, η_v strictly decreases with respect to p and strictly increases with respect to n. For $T \in [25{,}50]$ we have $\rho'(T) = 0.037564T - 2.0441 < 0$, $\nu'(T) < 0$ and $\rho, \nu > 0$; with negative powers, it follows that $\rho(T)^{-\frac{0.27}{0.73}}$ and $\nu(T)^{-\frac{0.54}{0.73}}$ strictly increase with respect to T, i.e.,η_v strictly decreases with respect to T. □

Appendix A.2. Stage (II)—Reduction and Global Optimality with Respect to (λ, r_c^*)

Reduction to a problem with respect to (λ, r_c^*) *at* $(p_{min}, n_{max}, T_{min})$. From Lemma A1, it follows that for a global maximum of η_v it is sufficient to fix $p_{min}, n_{max}, T_{min}$, and to maximize η_v with respect to (λ, r_c^*) in the feasible domain. This is equivalent to minimizing the negative multiplier:

$$P(\lambda, r_c^*) := u(\lambda, r_c^*; z)^{\gamma}K(\lambda, r_c^*; z) \tag{A9}$$

where $\gamma = 0.54 / 0.73 \approx 0.739726$, since $\eta_v = 1 - \text{const} \cdot P(\lambda, r_c^*)$ at fixed p, n, T.

Proof for the global maximum with respect to (λ, r_c^*) *in the feasible domain:* We introduce $\kappa = -\frac{1.27-1}{1.27-2} = 0.369863$. Since $\frac{1.27-1}{1.27-2} = -\kappa < 0$, it follows that $R^{\frac{1.27-1}{1.27-2}} = R^{-\kappa}$ and therefore K contains the multiplier R^{κ} in the numerator. Using $u = \frac{z+\lambda+2r_c^*}{d_{Hf}}$ and the equality $(\lambda + 2r_c^* + z) = ud_{Hf}$, the expressions are significantly simplified. For fixed $d_{Hf} = 57$, $b = 10$, $\delta_1 = \delta_2 = 0.012$, we obtain:

$$N = (3b\delta_1 + \delta_2\pi d_{Hf})u^2 + (4\delta_2)r_c^*u = a_Nu^2 + b_Nr_c^*u,$$

where the following substitutions are made: $a_N = 0.36 + 0.012 \cdot \pi \cdot 57 \approx 2.508$ and $b_N = 0.048$. and $R = \frac{A}{B}$, where

$$A = \left(12b\delta_1 + 4\delta_2\pi d_{Hf}\right)u^2 + (16\delta_2)r_c^* u = c_1 u^2 + c_2 r_c^* u,$$

$$B = \left(6b + 6\delta_1 + 8\delta_2 + 2\pi d_{Hf}\right)u + 8r_c^* = c_3 u + 8r_c^*,$$

$$c_1 \approx 10.035, \quad c_2 = 0.192, \quad c_3 \approx 418.308.$$

After substitution into (A4) we get:

$$K(\lambda, r_c^*; z) = \frac{(a_N u + b_N r_c^*)R(u, r_c^*)^{\kappa}}{b z^{1.11} L(\lambda, r_c^*)}, \tag{A10}$$

where $L(\lambda, r_c^*) = 476\lambda - 11r_c^* + 10$. Therefore, the negative multiplier in (A9) can be written as:

$$P(\lambda, r_c^*) = u^{\gamma} \frac{a_N u + b_N r_c^*}{L(\lambda, r_c^*)} R(u, r_c^*)^{\kappa} C_z, \tag{A11}$$

where $C_z = 1/(b z^{1.11}) > 0$. Since $C_z > 0$ is a constant for a fixed z, the monotonicities of P are determined by the remaining multipliers. Furthermore, from (29) it follows $\lambda \geq \frac{0.5}{\cos\left(\frac{1.15\pi}{z}\right)} \geq 0.5$, therefore $L(\lambda, r_c^*)$ is strictly positive for $r_c^* \leq 1.6$:

$$L(\lambda, r_c^*) \geq 476 \cdot 0.5 - 11 \cdot 1.6 + 10 = 230.4 > 0 \tag{A12}$$

Lemma A2. *(P strictly decreases with respect to λ at a fixed r_c^*). Let $r_c^* \in [0.5, 1.6]$ be fixed and (λ, r_c^*) be feasible from the set $(g_1 \leq 0, g_2 \leq 0)$. Then $P(\lambda, r_c^*)$ is a strictly decreasing function of λ in the feasible interval for λ. Therefore,η_v is strictly increasing with respect to λ.*

Proof. For a fixed r_c^* we have $u = \frac{z + \lambda + 2r_c^*}{d_{Hf}}$ and $\frac{du}{d\lambda} = \frac{1}{d_{Hf}} = 1/57$. From (A11) we write:

$$\ln P = \gamma \ln u + \ln(a_N u + b_N r_c^*) + \kappa \ln R\,(u, r_c^*) - \ln L\,(\lambda, r_c^*) + \text{const} \tag{A13}$$

Since $R(u, r_c^*) = \frac{u(c_1 u + c_2 r_c^*)}{c_3 u + 8r_c^*}$, we obtain:

$$\ln R = \ln u + \ln(c_1 u + c_2 r_c^*) - \ln(c_3 u + 8r_c^*) \tag{A14}$$

Differentiating (A13) with respect to λ and using (A14), we get:

$$\frac{d}{d\lambda} \ln P = \frac{1}{57} B(u, r_c^*) - \frac{476}{L(\lambda, r_c^*)}, \tag{A15}$$

where:

$$B(u, r_c^*) = \frac{\gamma}{u} + \frac{a_N}{a_N u + b_N r_c^*} + \kappa\left(\frac{1}{u} + \frac{c_1}{c_1 u + c_2 r_c^*} - \frac{c_3}{c_3 u + 8r_c^*}\right).$$

It can be seen that the last term in the parentheses is non-positive, since $\frac{c_3}{c_3 u + 8r_c^*} \geq 0$, thus yielding the following upper bound:

$$B(u, r_c^*) \leq \frac{\gamma}{u} + \frac{a_N}{a_N u + b_N r_c^*} + \kappa\left(\frac{1}{u} + \frac{c_1}{c_1 u + c_2 r_c^*}\right) \tag{A16}$$

Since $z \geq 4$, $\lambda \geq 0.5$ and $r_c^* \geq 0.5$, we have $u = \frac{z + \lambda + 2r_c^*}{57} \geq \frac{4 + 0.5 + 1}{57} = \frac{5.5}{57} \approx 0.09649$. Also $a_N u + b_N r_c^* \geq a_N \cdot 0.09649 + b_N \cdot 0.5 \approx 0.266$ and $c_1 u + c_2 r_c^* \geq c_1 \cdot 0.09649 + c_2 \cdot 0.5 \approx 1.064$.

Therefore:

$$B(u, r_c^*) \leq \frac{\gamma}{0.09649} + \frac{a_N}{0.266} + \kappa\left(\frac{1}{0.09649} + \frac{c_1}{1.064}\right) \approx 7.666 + 9.42 + 0.3699(10.36 + 9.43) < 25 \tag{A17}$$

Hence $\frac{1}{57} B(u, r_c^*) < \frac{25}{57} \approx 0.439$. On the other hand, $L(\lambda, r_c^*) \leq 476 \cdot 1 - 11 \cdot 0.5 + 10 = 480.5$, so that:

$$\frac{476}{L(\lambda, r_c^*)} \geq \frac{476}{480.5} \approx 0.991 \tag{A18}$$

Combining (A14), (A17), and (A18) we obtain $\frac{d}{d\lambda}\ln P \leq 0.439 - 0.991 < 0$ for all feasible (λ, r_c^*) from the feasible set. Therefore, $P(\lambda, r_c^*)$ strictly decreases with respect to λ at a fixed r_c^*, i.e.,$\eta_v = 1 - \text{const} \cdot P$ strictly increases with respect to λ. □

Corollary A1. *(Activity of the upper bound for* λ*): For any fixed* r_c^**, the optimal value of* λ *is the maximum feasible* λ*. In the set* $(g_1 \leq 0, g_2 \leq 0)$ *this yields:*

$$\lambda_{max}(r_c^*) = \min\left\{r_c^*, \left(1 - \alpha(z) r_c^{*2}\right)^{0.5}\right\}, \quad \text{(A19)}$$

where $\alpha(z) = \frac{4(z+1)^3}{27(z-1)z^2}$*. The intersection point* $r_{c,opt}^*$ *is the solution of* $r_c^* = \left(1 - \alpha(z) r_c^{*2}\right)^{0.5}$*, i.e.:*

$$r_{c,opt}^* = \left(\frac{1}{1+\alpha(z)}\right)^{0.5} = \left(\frac{27(z-1)z^2}{27(z-1)z^2 + 4(z+1)^3}\right)^{0.5} \quad \text{(A20)}$$

Lemma A3. *Let* $z \in \{4, \ldots, 17\}$ *be fixed and* $r_c^* \in [0.5, 1.6]$*. Let* $\alpha(z) = \frac{4(z+1)^3}{27(z-1)z^2}$ *and* $r_{c,opt}^* = \left(\frac{1}{1+\alpha(z)}\right)^{0.5}$*. We set:*

$$\lambda_{max}(r_c^*) = \min\left\{r_c^*, \sqrt{1 - \alpha(z) r_c^{*2}}\right\}, \quad \tilde{P}(r_c^*) = P(\lambda_{max}(r_c^*), r_c^*) \quad \text{(A21)}$$

Then $\tilde{P}(r_c^*)$ is strictly decreasing on $\left[0.5, r_{c,opt}^*\right]$ and strictly increasing on $\left[r_{c,opt}^*, 1.6\right]$. Therefore, $\tilde{P}(r_c^*)$ has a unique global minimum at $r_c^* = r_{c,opt}^*$, and $\eta_v = 1 - C\tilde{P}$ $(C > 0)$ has a global maximum at $\lambda = r_c^* = r_{c,opt}^*$.

Proof. Let $f(r_c^*) = \ln \tilde{P}(r_c^*)$. Since ln is strictly monotonic, $f'(r_c^*)$ and $\tilde{P}'(r_c^*)$ have the same sign. The following representation is used:

$$\ln P(\lambda, r_c^*) = \gamma \ln u + \ln(a_N u + b_N r_c^*) + \kappa \ln R(u, r_c^*) - \ln L(\lambda, r_c^*) + \text{const}, \quad \text{(A22)}$$

where $u = \frac{z+\lambda+2r_c^*}{57}$, $L(\lambda, r_c^*) = 476\lambda - 11 r_c^* + 10$, $\gamma = \frac{0.54}{0.73}$, $\kappa = 0.369863$, $R(u, r_c^*) = \frac{u(c_1 u + c_2 r_c^*)}{c_3 u + 8 r_c^*}$, and $a_N, b_N, c_1, c_2, c_3 > 0$ are constants. The envelope $\lambda = \lambda_{max}(r_c^*)$ has two branches. If $r_c^* \leq r_{c,opt}^*$, then $\lambda_{max}(r_c^*) = r_c^*$ (the constraint $\lambda \leq r_c^*$ is active). If $r_c^* \geq r_{c,opt}^*$, then $\lambda_{max}(r_c^*) = \sqrt{1 - \alpha(z) r_c^{*2}}$ (the constraint $\lambda^2 + \alpha(z) r_c^{*2} = 1$ is active).

(i) If $r_c^* \leq r_{c,opt}^*$, then $\lambda_{max}(r_c^*) = r_c^*$ and $L(r_c^*) = 465 r_c^* + 10$. Differentiating, we obtain:

$$f'(r_c^*) = A(r_c^*) - \frac{465}{465 r_c^* + 10} \quad \text{(A23)}$$

where $A(r_c^*)$ is the sum of the derivatives of the remaining three terms. For $z \in [4, 17]$, $r_c^* \in [0.5, 1]$. These derivatives are bounded from above, specifically $A(r_c^*) \leq 1.06$. On the other hand $\frac{465}{465 r_c^* + 10} \geq \frac{465}{475} \approx 0.979$. Therefore, $f'(r_c^*) < 0$ on $\left[0.5, r_{c,opt}^*\right]$ and$\tilde{P}(r_c^*)$ strictly decreases.

(ii) If $r_c^* \geq r_{c,opt}^*$, then $\lambda_{max}(r_c^*) = \sqrt{1 - \alpha(z) r_c^{*2}}$ and$\lambda'(r_c^*) = -\frac{\alpha(z) r_c^*}{\lambda} < 0$. Therefore:

$$L'(r_c^*) = 476\lambda'(r_c^*) - 11 < 0 \quad \text{and} \quad \frac{d}{dr_c^*}(-\ln L) = -\frac{L'}{L} = \frac{11 + 476|\lambda'(r_c^*)|}{L} > 0 \quad \text{(A24)}$$

The remaining terms in $f'(r_c^*)$ depend on r_c^* through $u'(r_c^*) = \frac{2+\lambda'(r_c^*)}{57}$ and have a growth of at most order $O(|\lambda'|)/57$, while the contribution from $-\ln L$ is of order $\frac{476|\lambda'|}{L}$ (a coefficient of order 1). Therefore, $f'(r_c^*) > 0$ for $r_c^* \geq r_{c,opt}^*$ and $\tilde{P}$ strictly increases. Combining (i) and (ii), we obtain that $\tilde{P}$ decreases up to $r_{c,opt}^*$ and increases thereafter, i.e., it has a unique global minimum at $r_c^* = r_{c,opt}^*$. □

Theorem A1. *(Global maximum of* η_v *in the feasible domain). For fixed* $z \in \{4, \ldots, 17\}$ *and fixed* d_{Hf}*, b,* δ_1*,* δ_2*, in the extended set* $(g_1 \le 0,\ g_2 \le 0, 0 \le \lambda \le 1, 0.5 \le r_c^* \le 1.6)$*, the single-objective problem* $\max\{\eta_v\}$ *has a global maximum at the point:*

$$(\lambda, r_c^*, p, n, T) = \left(r_{c,opt}^*, r_{c,opt}^*, p_{min}, n_{max}, T_{min}\right) \tag{A25}$$

Since the real feasible set is a subset of the extended one, and the point (67) is feasible for it as well, the same point is also a global maximum for the original problem. The proof of Theorem A1 is a direct consequence of the proven lemmas.

We will provide (without proof) a theorem for the global maximum of $Q(X)$. The proof of Theorem A2 is similar to that of Theorem A1.

Theorem A2. *(Global maximum of* $Q(X)$ *in the extended set). For fixed* $z \in \{4, \ldots, 17\}$ *and fixed* d_{Hf}*, b,* δ_1*,* δ_2*, in the extended set* $(g_1 \le 0,\ g_2 \le 0, 0 \le \lambda \le 1, 0.5 \le r_c^* \le 1.6)$*, the single-objective problem* $\max\{Q(X)\}$ *has a global maximum at the point:*

$$(\lambda, r_c^*, p, n, T) = \left(r_{c,opt}^*, r_{c,opt}^*, p_{min}, n_{max}, T_{min}\right), \tag{A26}$$

Since the real feasible set is a subset of the extended one, and the point (A26) is feasible for it as well, the same point is also a global maximum for the original problem. From Theorem A1 and Theorem A2, it follows that the two criteria taken separately do not contradict each other, and their global maximums are at the same point in the feasible domain. This means that we can formulate the following fundamental statement, which is important for the study:

Theorem A3. *For fixed* $z \in \{4, \ldots, 17\}$ *and fixed* d_{Hf}*,* b*,* δ_1*,* δ_2*, in the extended set* $(g_1 \le 0, g_2 \le 0{,}0 \le \lambda \le 1{,}0.5 \le r_c^* \le 1.6)$*, the bi-objective problem* $\max\{Q(X)\}$ *and*$\max\{\eta_v\}$ *has a global maximum at the same point for both criteria:*

$$(\lambda, r_c^*, p, n, T) = \left(r_{c,opt}^*, r_{c,opt}^*, p_{min}, n_{max}, T_{min}\right). \tag{A27}$$

Theorem A4. *(Bounds on the parameters* B_1 *and* w *for preserving the conflict with respect to* z*). Let the exponent* w *in the generalized criterion equation of the volumetric efficiency not be fixed in advance, but be considered as a parameter:*

$$\eta_v = 1 - B_1 \mu^* \left(\frac{\pi_1}{\pi_2^w}\right)^{\frac{1}{2-w}} K_w, \tag{A28}$$

where

$$K_w = \frac{S_n^* (d_s^*)^\kappa}{q^*}, \qquad \kappa = \frac{w-1}{2-w}. \tag{A29}$$

Then, from the requirement that the proofs of Lemma A2 and Lemma A3 preserve the same sign structure after replacing the calibrated value $w = 1.27$ with a general parameter w, the following sufficient bounds are obtained:

$$B_1 > 0, \qquad 1 < w < w_0, \qquad w_0 \approx 1.304. \tag{A30}$$

Consequently, in a conservatively rounded form, the statement concerning the structural conflict between the actual flow rate Q and the volumetric efficiency η_v with respect to the number of teeth z remains valid for

$$B_1 > 0, \qquad 1 < w < 1.30. \tag{A31}$$

Under these conditions, the specific values of B_1 and w influence the quantitative level of the losses and the exact position of the compromise choice of z, but they do not generate the conflict itself between flow rate and efficiency.

https://doi.org/10.3390/machines14070720

Proof. In the reduction used in Appendix A, the maximization of η_v for fixed p, n, T is reduced to the minimization of a positive geometric loss multiplier. For a general exponent w, this can be written in the form

$$\eta_v = 1 - C_w P_w(\lambda, r_c^*), \quad C_w = B_1 \mu^* \left(\frac{\pi_1}{\pi_2^w}\right)^{\frac{1}{2-w}}. \tag{A32}$$

In the physically admissible domain, we have $\mu^* > 0$, $\pi_1 > 0$, and $\pi_2 > 0$. Therefore, the sign of C_w is determined only by the sign of B_1. In order for the maximization problem for η_v to remain equivalent to a minimization problem forP_w, as in the proof of Lemma A2 and Lemma A3, it is necessary that

$$C_w > 0 \Leftrightarrow B_1 > 0. \tag{A33}$$

If $B_1 = 0$, the loss term disappears and the efficiency problem degenerates; if $B_1 < 0$, the sign of the loss term is reversed and a different, physically inadmissible optimization problem is obtained. Therefore, the condition $B_1 > 0$ is not imposed in advance, but follows from the sign required for the proof itself.

With respect to w, we introduce

$$\kappa = \frac{w-1}{2-w}, \qquad \gamma = 2\kappa. \tag{A34}$$

Since, in the proof, the geometric factor contains positive power multipliers of the formR^{κ}, the first necessary sign condition is $\kappa > 0$. This gives

$$\frac{w-1}{2-w} > 0 \Rightarrow 1 < w < 2. \tag{A35}$$

Consequently, the lower bound $w > 1$ is also obtained from the requirement of preserving the proof structure, and is not adopted in advance.

It remains to estimate the upper bound. Repeating the estimates from Lemma A2 with a general parameter κ, we obtain a condition of the form

$$\frac{1}{57} B_\kappa(u, r_c^*) - \frac{476}{L(\lambda, r_c^*)} < 0, \tag{A36}$$

where B_κ is the corresponding upper estimate of the logarithmic derivative of P_w with respect to λ. Substitution of the constants from (A13)–(A18) shows that this condition remains satisfied for approximately

$$\kappa < \kappa_1 \approx 1.16. \tag{A37}$$

Therefore, Lemma A2 does not provide the strictest bound. The restriction is obtained from Lemma A3. Along the first branch of the active boundary $\lambda_{max}(r_c^*) = r_c^*$, the logarithmic derivative has the form

$$f_w'(r_c^*) = A_\kappa(r_c^*, z) - \frac{465}{465 r_c^* + 10}. \tag{A38}$$

In order to preserve the sign $f_w'(r_c^*) < 0$ on $[0.5, r_{c,opt}^*]$ and, respectively, the sign $f_w'(r_c^*) > 0$ along the second branch $\lambda_{max}(r_c^*) = \sqrt{1 - \alpha(z) r_c^{*2}}$, the terms containing κ must remain smaller than the stabilizing contribution of the term $-\ln L$. The numerical evaluation of these inequalities over the compact domain $z \in \{4, \dots, 17\}, r_c^* \in [0.5, 1.6]$ gives the strictest sufficient bound

$$\kappa < \kappa_0 \approx 0.437. \tag{A39}$$

Since$\kappa_0 < \kappa_1$, it is precisely (A39) that is the limiting condition. From the relation $\kappa = (w-1)/(2-w)$ it follows that

$$w = \frac{1+2\kappa}{1+\kappa}. \tag{A40}$$

Consequently, for $\kappa = \kappa_0 \approx 0.437$ we obtain

$$w_0 = \frac{1+2\kappa_0}{1+\kappa_0} \approx \frac{1+2\cdot 0.437}{1+0.437} \approx 1.304. \tag{A41}$$

https://doi.org/10.3390/machines14070720

Thus, from the sign estimates in the proof themselves, the following sufficient bounds follow:

$$B_1 > 0, \qquad 1 < w < 1.304. \tag{A42}$$

By conservatively rounding the upper bound, we obtain the convenient interval $1 < w < 1.30$.

Under these conditions, the proofs of Lemma A2 and Lemma A3 preserve their signs; therefore, the minimum of the geometric loss multiplier remains at the same point

$$\lambda = r_c^* = r_{c,opt}^*. \tag{A43}$$

On the other hand, the theoretical flow rate $Q_t = qn$ depends on the working displacement q and the frequency n, and, for fixed external dimensions, the dependence of q on the number of teeth z is geometric and contains neither B_1 nor w. The parameters B_1 and w enter only through the loss multiplier inη_v and, accordingly, change the numerical level of $Q = Q_t\eta_v$, but do not change the reason for the opposite tendencies with respect to z.

Therefore, for $B_1 > 0$ and $1 < w < 1.30$, a smaller number of teeth favors the working displacement and the flow rate, whereas a larger number of teeth reduces the relative leakages and increases the volumetric efficiency. The conflict between Q and η_v with respect to z remains a structural-geometric property of the considered class of pumps, and not an artifact of the specific experimental calibration of B_1 and $w = 1.27$. □

Remark. *The number* $w_0 \approx 1.304$ *is not claimed to be an exact necessary bound. It is a sufficient bound obtained from the theorems, lemmas, and derivative estimates used. Therefore, it is more appropriate to use the conservative interval* $1 < w < 1.30$.

References

1. Cieślicki, R.; Karpenko, M. An Investigation of the Impact of Pump Deformations on Circumferential Gap Height as a Factor Influencing Volumetric Efficiency of External Gear Pumps. *Transport* **2022**, *37*, 373–382. https://doi.org/10.3846/transport.2022.18331.
2. Urbanowicz, K.; Bergant, A.; Stosiak, M.; Deptuła, A.; Karpenko, M. Navier-Stokes Solutions for Accelerating Pipe Flow—A Review of Analytical Models. *Energies* **2023**, *16*, 1407. https://doi.org/10.3390/en16031407.
3. EnginSoft. Newsletter Year 14 n°1: How to Optimize an External Gear Pump in Highly Constrained Conditions. Available online: https://www.enginsoft.com/assets/pdf/newsletter/newsletter2017-1-casappa.pdf (accessed on 22 April 2026).
4. Vacca, A.; Guidetti, M. Modelling and experimental validation of external spur gear machines for fluid power applications. *Simul. Model. Pract. Theory* **2011**, *19*, 2007–2031. https://doi.org/10.1016/j.simpat.2011.05.009.
5. Ivantysyn, J.; Ivantysynova, M. *Hydrostatic Pumps and Motors*; Tech Books International: New Delhi, India, 2001.
6. Torrent, M.; Gamez-Montero, P.J.; Codina, E. Motion Modelling of the Floating Bushing in an External Gear Pump Using Dimensional Analysis. *Actuators* **2023**, *12*, 338.
7. Popov, G.; Klimentov, K.; Kostov, B.; Dimitrova, R. Analyzing the Energy Efficiency of Fan Systems by Using the Dimensional Analysis (DA) Method. *Symmetry* **2020**, *12*, 537.
8. Klimentov, K.; Legutko, S.; Popov, G.; Kostov, B. Applying Criteria Equations in Studying the Energy Efficiency of Pump Systems. *Energies* **2021**, *14*, 5256.
9. Ospina, Á.; Herrera Ríos, E.; Jaramillo, J.; Franco, C.A.; Taborda, E.A.; Cortes, F.B. Integrating Dimensional Analysis and Machine Learning for Predictive Maintenance of Francis Turbines in Sediment-Laden Flow. *Energies* **2025**, *18*, 4023.
10. Nikolaev, I.; Georgiev, I.; Georgiev, S.; Iliev, G. Numerical investigation of the actual volumetric flow rate and volumetric efficiency and optimization of the geometric parameters of a three-rotor pump with lantern meshing—Part I. *Machines* **2026**, *14*, 591.
11. Gonçalves, M.L.N.; Lima, F.S.; Prudente, L.F. Globally convergent Newton-type methods for multiobjective optimization. *Comput. Optim. Appl.* **2022**, *83*, 403–434. https://doi.org/10.1007/s10589-022-00414-7.
12. Fliege, J.; Svaiter, B. Steepest descent methods for multicriteria optimization. *Math. Methods Oper. Res.* **2000**, *51*, 479–494. https://doi.org/10.1007/s001860000043.

13. Désidéri, J.-A. Multiple-gradient descent algorithm (MGDA) for multiobjective optimizatio. *Comptes Rendus Math.* **2012**, *350*, 313–318. https://doi.org/10.1016/j.crma.2012.03.014.
14. Fliege, J.; Drummond, L.M.G.; Svaiter, B.F. Newton's Method for Multiobjective Optimization. *SIAM J. Optim.* **2009**, *20*, 602–626. https://doi.org/10.1137/08071692X.
15. Kumar, K.; Ghosh, D.; Upadhayay, A.; Yao, J.C.; Zhao, X. Quasi-Newton methods for multiobjective optimization problems: A systematic review. *Appl. Set-Valued Anal. Optim.* **2023**, *5*, 291–321. https://doi.org/10.23952/asvao.5.2023.2.12.
16. Povalej, Ž. Quasi-Newton's method for multiobjective optimization. *J. Comput. Appl. Math.* **2014**, *255*, 765–777. https://doi.org/10.1016/j.cam.2013.06.045.
17. Cocchi, G.; Liuzzi, G.; Lucidi, S.; Sciandrone, M. On the convergence of steepest descent methods for multiobjective optimization. *Comput. Optim. Appl.* **2020**, *77*, 1–27. https://doi.org/10.1007/s10589-020-00192-0.
18. Liu, X.; Reynolds, A.C. A multiobjective steepest descent method with applications to optimal well control. *Comput. Geosci.* **2016**, *20*, 355–374. https://doi.org/10.1007/s10596-016-9562-7.
19. Ghafariasl, P.; Mahmoudan, A.; Mohammadi, M.; Nazarparvar, A.; Hoseinzadeh, S.; Fathali, M.; Chang, S.; Zeinalnezhad, M.; Garcia, D.A. Neural network-based surrogate modeling and optimization of a multigeneration system. *Appl. Energy* **2024**, *364*, 123130. https://doi.org/10.1016/j.apenergy.2024.123130.
20. Sun, G.; Wang, S. A review of the artificial neural network surrogate modeling in aerodynamic design. *Proc. Inst. Mech. Eng. Part G J. Aerosp. Eng.* **2019**, *233*, 5863–5872. https://doi.org/10.1177/0954410019864485.
21. Zhang, X.; Xie, F.; Ji, T.; Zhu, Z.; Zheng, Y. Multi-fidelity deep neural network surrogate model for aerodynamic shape optimization. *Comput. Methods Appl. Mech. Eng.* **2021**, *373*, 113485. https://doi.org/10.1016/j.cma.2020.113485.
22. Viana, F.A.C.; Gogu, C.; Goel, T. Surrogate modeling: Tricks that endured the test of time and some recent developments. *Struct. Multidiscip. Optim.* **2021**, *64*, 2881–2908. https://doi.org/10.1007/s00158-021-03001-2.
23. Araújo, G.R.; Gomes, R.; Gomes, M.G.; Guedes, M.C.; Ferrão, P. Surrogate models for efficient multi-objective optimization of building performance. *Energies* **2023**, *16*, 4030. https://doi.org/10.3390/en16104030.
24. Bhosekar, A.; Ierapetritou, M. Advances in surrogate based modeling, feasibility analysis, and optimization: A review, *Comput. Chem. Eng.* **2018**, *108*, 250–267. https://doi.org/10.1016/j.compchemeng.2017.09.017.
25. Tripathy, R.K.; Bilionis, I. Deep UQ: Learning deep neural network surrogate models for high dimensional uncertainty quantification, *J. Comput. Phys.* **2018**, *375*, 565–588. https://doi.org/10.1016/j.jcp.2018.08.036.
26. Dimov, I.; Maire, S.; Todorov, V. An unbiased Monte Carlo method to solve linear Volterra equations of the second kind. *Neural Comput. Applic.* **2022**, *34*, 1527–1540. https://doi.org/10.1007/s00521-021-06417-5.
27. Dimov, I.; Todorov, V.; Sabelfeld, K. A study of highly efficient stochastic sequences for multidimensional sensitivity analysis. *Monte Carlo Methods Appl.* **2022**, *28*, 1–12. https://doi.org/10.1515/mcma-2022-2101.
28. Todorov, V.; Dimov, I.; Ostromsky, T.; Zlatev, Z.; Georgieva, R.; Poryazov, S. Optimized Quasi-Monte Carlo Methods Based on Van der Corput Sequence for Sensitivity Analysis in Air Pollution Modelling. In *Recent Advances in Computational Optimization*; Studies in Computational Intelligence; Springer: Cham, Switzerland, 2022; Volume 986. https://doi.org/10.1007/978-3-030-82397-9_20.
29. Todorov, V.; Dimov, I. Efficient Stochastic Approaches for Multidimensional Integrals in Bayesian Statistics. In *Large-Scale Scientific Computing*; Lecture Notes in Computer Science; Springer: Cham, Switzerland, 2020; Volume 11958. https://doi.org/10.1007/978-3-030-41032-2_52.
30. Saltelli, A.; Tarantola, S.; Campolongo, F.; Ratto, M. *Sensitivity Analysis in Practice: A Guide to Assessing Scientic Models*; Halsted Press: New York, NY, USA, 2004.
31. Sobol, I.M. *Monte Carlo Numerical Methods*; Nauka: Moscow, Russia, 1973.
32. Jindra, D.; Kala, Z.; Kala, J. Two Stochastic Methods to Model Initial Geometrical Imperfections of Steel Frame Structures. *Buildings* **2024**, *14*, 196.
33. Miettinen, K. *Nonlinear Multiobjective Optimization*, 1st ed.; Springer: New York, NY, USA, 1998.
34. Ehrgott, M. *Multicriteria Optimization*, 2nd ed.; Springer: Berlin/Heidelberg, Germany, 2005.
35. Bonami, P.; Biegler, L.T.; Conn, A.R.; Cornuéjols, A.; Grossmann, I.E.; Laird, C.D.; Lee, J.; Lodu, A.; Margot, F.; Sawaya, N.; et al. An algorithmic framework for convex mixed integer nonlinear programs. *Discret. Optim.* **2008**, *15*, 186–204.
36. Tawarmalani, M.; Sahinidis, N.V. *Convexification and Global Optimization in Continuous and Mixed-Integer Nonlinear Programming*, 1st ed.; Springer: New York, NY, USA, 2002.
37. Vigerske, S. MINLP Solver Technology. 2017. Available online: https://www.gams.com/~svigerske/2017_minlp.pdf (accessed on 9 March 2026).

38. Duran, M.A.; Grossmann, I.E. An outer-approximation algorithm for a class of mixed-integer nonlinear programs. *Math. Program.* **1986**, *36*, 307–339.
39. Deb, K.; Pratap, A.; Agarwal, S.; Meyarivan, T. A fast and elitist multi-objective genetic algorithm: NSGA-II. *IEEE Trans. Evol. Comput.* **2002**, *6*, 182–197.
40. Jaber, A.; Younes, R.; Lafon, P.; Khoder, J. A review on multi-objective mixed-integer non-linear optimization programming methods. *Eng* **2024**, *5*, 1961–1979.
41. Tuy, H. *Convex Analysis and Global Optimization*; Springer: Cham, Switzerland, 2016.
42. Yang, H.; Jang, H.S.; Ji, S. Volumetric efficiency prediction of external gear pumps using a leakage model based on dynamic clearances. *Actuators* **2026**, *15*, 56.
43. Torrent, M.; Gamez-Montero, P.J.; Codina, E. Parameterization, modeling, and validation in real conditions of an external gear pump. *Sustainability* **2021**, *13*, 3089.
44. Chiavola, O.; Frattini, E.; Palmieri, F.; Fioravanti, A.; Marani, P. On the efficiency of mobile hydraulic power packs operating with new and aged eco-friendly fluids. *Energies* **2023**, *16*, 5681.
45. Zardin, B.; Natali, E.; Borghi, M. Evaluation of the hydro-mechanical efficiency of external gear pumps. *Energies* **2019**, *12*, 2468.
46. Rundo, M. Models for flow rate simulation in gear pumps: A review. *Energies* **2017**, *10*, 1261.
47. Draganov, I.; Vitliemov, V.; Angelov, Y.; Mileva, S.; Ferdinandov, N.; Gospodinov, D.; Radev, R. Multi-criteria calibration of a thermo-mechanical model of steel plate welding in vacuum. *J. Manuf. Mater. Process.* **2024**, *8*, 225.
48. Sobol, I.M.; Statnikov, R.B. *Vybor Optimal'nykh Parametrov v Zadachakh co Mnogimi Kriternyami*; Drofa: Moscow, Russia, 2006.
49. Statnikov, R.B.; Matusov, I.B. *Mnogokriterial'noe Proektirovanie Mashin*; Mathematics/Cybernetics Series, No. 5; Znanie: Moscow, Russia, 1989.
50. Salukvadze, M.E. *Vector-Valued Optimization Problems in Optimal Control Theory*, 2nd ed.; Academic Press: New York, NY, USA, 2012.
51. Nikolaev, I. Volumetric displacement of a hydraulic machine with bilateral lantern meshing. *Toplotehnika* **2014**, *5*, 46–52. Available online: https://www.researchgate.net/publication/403537883 (accessed on 22 April 2026).
52. Yordanov, S.; Mihalev, G.; Ormandzhiev, K.; Ivanov, S. Application of a Modified Multiparametric PID Controller for Control of an Electrohydraulic Servo System. In *Proceedings of the 2024 International Conference Automatics and Informatics (ICAI)*; IEEE: Piscataway, NJ, USA, 2024; pp. 598–603.
53. Mihalev, G.; Yordanov, S.; Ormandzhiev, K.; Stoycheva, H.; Todorov, T. Synthesis of Model Predictive Control for an Electrohydraulic Servo System Using Orthonormal Functions. In *Proceedings of the 2024 5th International Conference on Communications, Information, Electronic and Energy Systems (CIEES)*; IEEE: Piscataway, NJ, USA, 2024; pp. 1–6.
54. Yordanov, S.; Mihalev, G.; Ormandzhiev, K.; Stoycheva, H. Synthesis of a MIMO Model of an Electro-Hydraulic System with Temperature Compensation. In *Proceedings of the 2025 International Conference Automatics and Informatics (ICAI)*; IEEE: Piscataway, NJ, USA, 2025; pp. 395–402.